Pro Gradu

Conductivity measurements of DNA TX tile and origami structures

Seppo-Tapio Paasonen

19th July 2011

UNIVERSITY OF JYVÄSKYLÄ
NANOSCIENCE CENTER
DEPARTMENT OF PHYSICS
MOLECULAR ELECTRONICS AND PLASMONICS

Preface

The work reported in this Master's thesis has been carried out between June 2008 and April 2010 at Nanoscience Center at the Department of Physics in the University of Jyväskylä.

First of all, I would like to thank my supervisor Dr. Jussi Toppari who has been a great mentor, friend, and help in the experimental part. I really feel that this opportunity You gave me was one the best things that have ever happened to me. I was honored to work in your guidance in the Nanoelectronics and Plasmonics group.

Secondly, Dr. Veikko Linko deserves my biggest thanks since he has been the one to teach me almost everything I know about DNA nanotechnology and experimental methods. Plus, I really appreciate our friendship.

The working atmosphere at the Nanoscience Center has been enjoyable altogether. Yet, I would like to emphasize the company of Mr. Mikko Palosaari, Mr. Olli Herranen, Mr. Antti Juutilainen, Mr. Johan Lindgren and Mr. Boxuan Shen. Your colorful company kept me going under all the stress. Many of you were of great assistance, so I thank you for your support.

I am in great debt to my grandparents who supported me financially, and whose believe in me never wavered.

Hämeenlinna 19th July 2011

Seppo-Tapio Paasonen

Abstract

This thesis is about DC and AC conductivity measurements performed on single self-assembled DNA constructs: a rectangular two-dimensional DNA slab fabricated via origami method and a wire-like construct via tile method. The sizes of these structures are roughly 70x100 nm^2 and 10×60 nm^2, respectively. In the field of molecular electronics the conductivity of DNA is a crucial question, and it is of great concern since DNA is a very promising molecule in a context of bottom-up based nanodevices due to its superior self-assembly properties. The structures are immobilized in nanoscale by using dielectrophoretic trapping to force the structures between two fingertip type nanoelectrodes where they attach to gold via thiol-Au bonding. Simple DC measurements in dry conditions revealed that the structures are good dielectrics, but AC measurements carried out in high humidity conditions revealed that adsorbed water molecules surrounding the DNA have a significant influence to the observed conductance.

List of Abbreviations

1D,2D,3D	one-dimensional, two-dimensional, three-dimensional
λ-DNA	a 48,502-base-pair-long dsDNA estracted from a virus *Phage Lambda*
σ-RH	conductivity versus relative humidity
A	adenine
AFM	atomic force microscopy
AC	alternating current
bp	base pair
C	cytosine
C6	hexane
CNT	carbon nanotube
CPE	constant phase element
CT	charge transfer
ctr	charge transfer resistance
DAE	double crossover, antiparallel, even spacing
DAC	digital-to-analog converter
DAO	double crossover, antiparallel, odd spacing
DAQ	data aquisition
DC	direct current
DFT	Density functional theory
DL	double layer
DX	double crossover
DEP	dielectrophoresis
DNA	deoxyribonucleic acid
dNTP	deoxynucleoside triphosphate
DPTA	dithiol-phosphoramidite
dsDNA	double-stranded DNA
EDTA	ethylenediaminetetraacetic acid
EIS	electrochemical impedance spectroscopy
EMS	electromagnetically shielded
G	guanine
GPIB	general-purpose interface bus
HAc	acetic acid
Hepes	2-[4-(2-hydroxyethyl)piperazin-1-yl]ethanesulfonic acid

HPLC	a purification method based on high performance liquid chromatography
I-RH	current versus relative humidity
I-V	current versus voltage
IHP	inner Helmholtz plane
IBT	Institute of Biomedical Technology - University of Tampere
iep	isoelectric point
IPA	isopropanol
IS	impedance spectroscopy
kb	kilobase
LUMO	lowest unoccupied molecular orbital
MgAc	magnesium acetate
MIBK	methyl isobutyl ketone
NSC	Nanoscience Center of University of Jyväskylä, Finland
nt	nucleotide
OHP	outer Helmholtz plane
PAGE	a purification method based on polyacrylamide gel electrophoresis
PCR	polymerase chain reaction
PMMA	polymethyl methacrylate
PZC	point of zero charge
pUC18	a 2,686-base-pair-long circular plasmid dsDNA from a bacterium *E.coli*
RC	resistor-capacitor
RH	relative humidity
SA	self-assembly
SEM	scanning electron microscope
SL	Stern layer
ssDNA	single-stranded DNA
T	thymine
TAE	Tris-acetate-EDTA
Tris	2-amino-2-hydroxymethyl-propane-1,3-diol
TX	triple crossover
UHV	ultra-high vacuum
ZP	zeta potential

Contents

Introduction

Strength of humankind has always come from the ability to identify, use, and modify materials and substances in ways that benefit us. The technological progress has been largely based on digital electronics, semiconductor technology, and the art of miniaturization through improved top-down fabrication methods. Modern chips have transistor densities so high that the transistor size might soon reach the atomic scale which for now is the ultimate barrier. So, semiconductor industry is already operating within nanoscale. Semiconductors are quite simple in composition, which is the reason why their properties cannot be modified beyond certain extend. Thus the point of nanotechnology, besides making use of the nanoscale phenomena, is to find new, more complex materials with new properties, ways to make something concrete out of those, and combine them with the existing technologies without losses in the density. Of course, the aim is to further increase it.

Quite obviously life is the most complex thing on this planet, and consequently organic molecules are typically much more complex than the inorganic. Luckily, the synthesis of organic molecules has taken a leap into a new era, which has given us the opportunity to create organic molecules and materials that could even replace the inorganic ones. In order to create something out of them, or of other common blocks of nanotechnology, one has to find ways to organize them in nanoscale. The bottom-up approaches which are typically based on self-assembly properties (SA) of molecules, have proven usable despite all difficulties. However, not all basic blocks or molecules of nanotechnology we would like to use have the properties needed. DNA is a unique molecule with properties unraveled by the evolution itself.

In this thesis conductive properties of two nanoscale DNA structures fabricated via two different approaches, origami and tile approaches, are studied. Getting information about possible conduction mechanisms is important because many mechanisms have been proposed, and because DNA structures could be used as nanoscale breadboards or even as components of molecular electronics in future nanoscale systems.

Chapter 1 is mainly theoretical: First, the basic concepts of DNA are introduced, which is essential to understanding the fundamentals of DNA constructs and conductivity. Dielectrophoresis is presented next, as it is the tool used in this thesis to immobilize the structures in nanoscale. Finally, the principles of impedance spectroscopy are considered to gain the basic knowledge required to analyze the AC spectra. The experimental methods used are described in more detail in chapter 2 (and appendices). All the main results obtained are presented and analysed in detail in chapter 3.

Chapter 1

Background

1.1 Natural DNA

1.1.1 Structure, properties, conformations

DNA can be found on each living cell in form of chromosomes which have organized into pairs inside a nucleus so that both of the chromosomes are almost identical. DNA is divided into sequences in such a way that between the sequences it has wrapped twice around a protein. If the proteins are removed, a long DNA thread is obtained. The thread consists of two long polymers of deoxyribonucleotides (ssDNA) bound to each other in a specific way so that they form a double helix (figure 1.1).

Each nucleotide contains a deoxyribose sugar, a phosphate, and one of four aromatic nitrogenous bases attached to the sugar. The four bases are Thymine (T), Cytosine (C), Adenine (A), and Guanine (G) (figure 1.2b). T and C are single-ring structures called pyrimidines, whereas A and G are larger double-ring structures called purines. The phosphate and sugar groups form the backbone of ssDNA to which the bases are attached (figure 1.2a). The backbone is not quite symmetric but it has directionality. The so-called 3' and 5' ends are determined by the carbon atom of the sugar on which the phosphate is attached.

The bases bind to each other forming pairs through hydrogen bonding. James Watson and Francis Crick proposed in 1953 [1] that the most stable base pairs are A-T with two hydrogen bonds and G-C with three bonds (figure 1.2b), which leads to the property called complementarity. Double-stranded DNA (dsDNA, figure 1.2c) is formed of two ssDNA sequences held together by the hydrogen bonds between the complementary bases, van der Waals forces, and dipole-dipole interactions. The helix is about 2 nm wide (figure 1.2c), and the hydrophobic bases are in
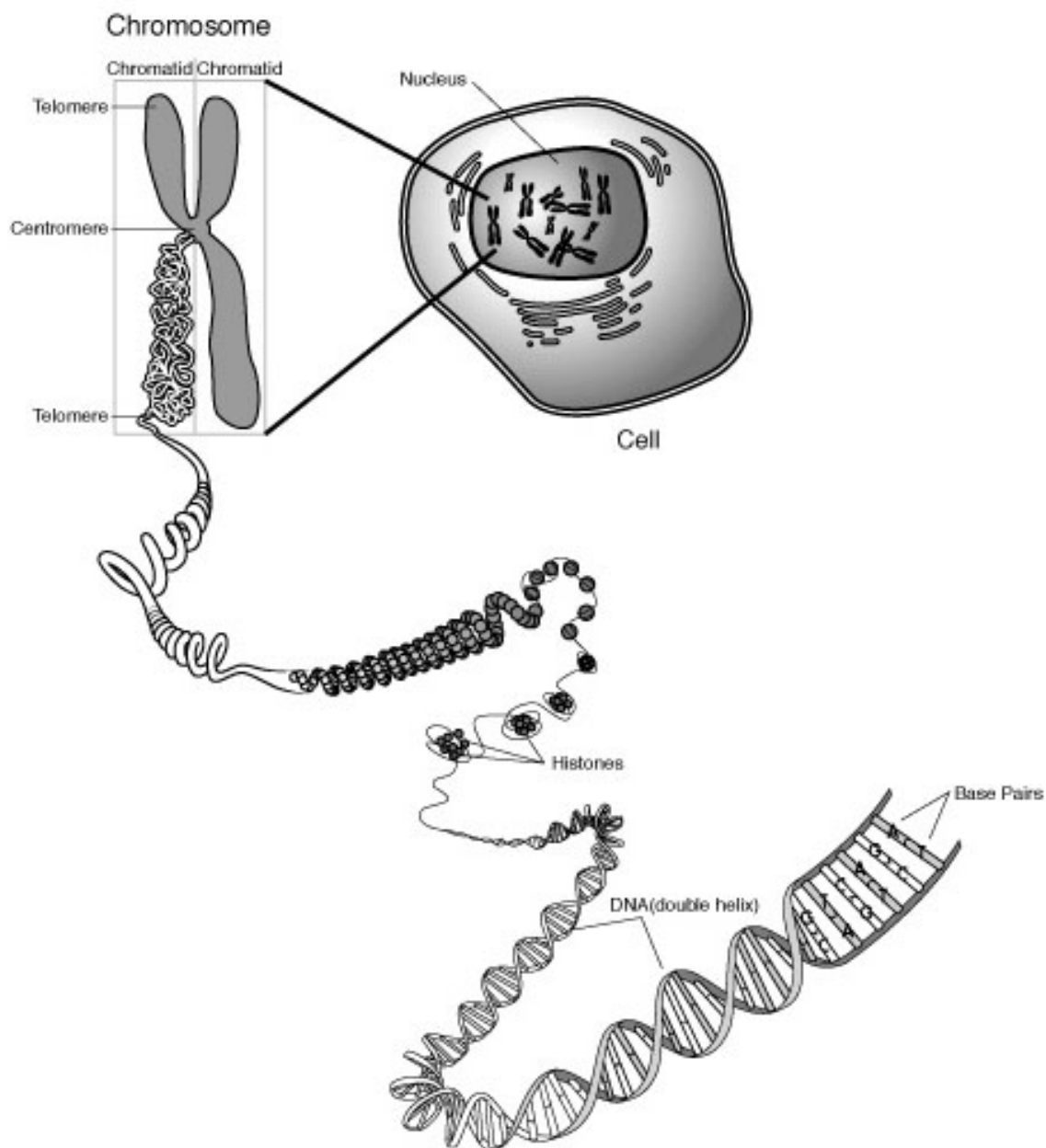
Figure 1.1: *DNA inside a nucleus.*

the center of the helix. In addition, the single strands are antiparallel to each other with respect to the coordination of the phosphodiester bonds, and the environment has a huge impact on the stability of the double strand.

Double-stranded DNA can have many possible conformations depending on the sequence, chemical modifications of the bases, solution conditions, and possible supercoiling. In living organisms the so-called A-DNA, B-DNA, and Z-DNA forms have been observed (figure 1.3). Yet many other more exotic conformations exist,

Figure 1.2: *a) The structure of ssDNA. b) Hydrogen bonding between bases. c) DNA double helix.*

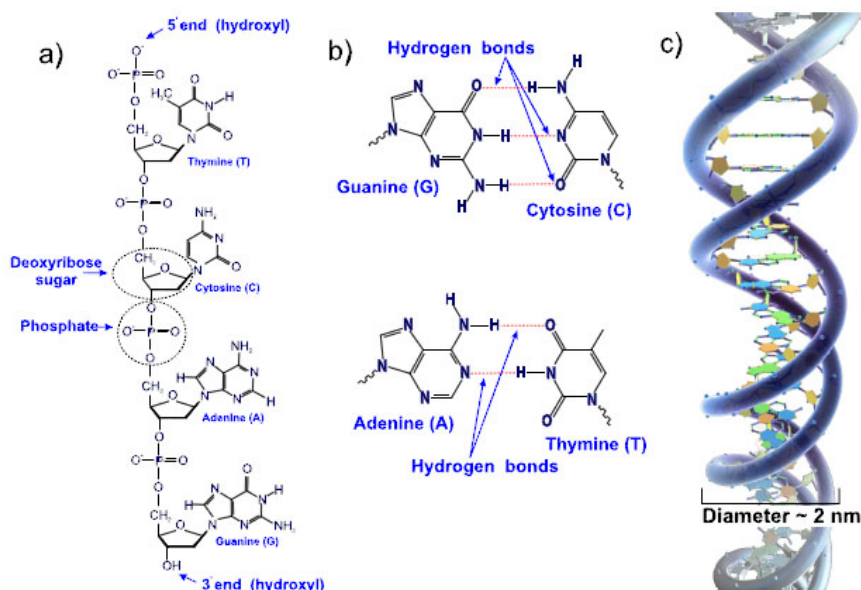e.g. H triplex and G tetraplex conformations which form through Hoogsten pairing [2,3]. The relaxed B-DNA is the most common conformation found in the cells of living organisms as it is the most stable structure for a random-sequenced DNA molecule under natural conditions. The Hoogsten pairing typically requires homogeneous sequences, and in some triplex cases low pH since one of the nitrogens in C or A must be protonated [4]. The G tetraplexes are typically further stabilized by monovalent cations [5].

In B-DNA the center of the base pairs (bp) lies along the helix axis. The helix is right-handed and the separation of the bp is about 3.4 Å while they are slightly tilted. There are about 10.5 bp per each turn of the helix, which yields an angle of 36º between successive pairs. B-DNA requires more than 13 water molecules per nucleotide to remain stable. The other right-handed conformation, A-DNA, is a little bit wider and requires only 5-10 water molecules per nucleotide. It has approximately 11 bp per turn. The Z-DNA is left-handed, has adopted a zigzag configuration, and has about 12 bp per turn. [4]
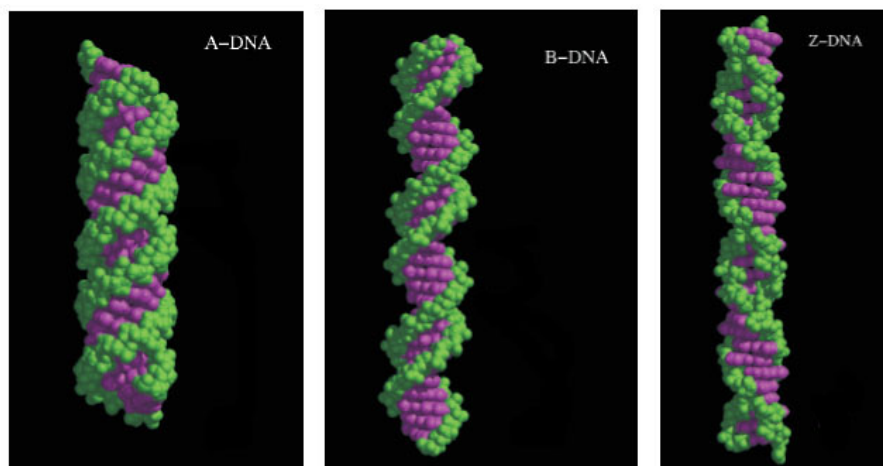
Figure 1.3: *The most common conformations of DNA. The backbone is in green and violet desbribes the bases.*

1.1.2 Fabrication methods of DNA

Fragments of nucleic acids with defined chemical structure, oligonucleotides, can be produced synthetically. Currently, the process is implemented as solid-phase synthesis using a phosphoramidite method, i.e. the basic building blocks in this method are nucleoside phosphoramidites. The building blocks are sequentially coupled to the growing chain in the order required. The process has been fully automated since the late 1970s and is commercially available. The occurence of side reactions sets practical limits for the length of synthetic oligonucleotides. The synthesis also allows adding functional groups to the oligonucleotides. [6, 7]

Restriction enzymes can be used to cut DNA at specific recognition nucleotide sequences known as restriction sites which are typically palindromic. Each enzym has its own recognition sequence and way to make the cut. The name comes from the fact that inside a bacterial host the restriction enzymes selectively cut up foreign DNA and thus provide a defence mechanism against viruses. Hundreds of enzymes are commercially available and are widely used for DNA modification and manipulation. [8]

Replication of DNA is done via polymerase chain reaction (PCR). The method exponentially amplifies a chosen sequence from a template and is based on a DNA polymerase, i.e. an enzyme that catalyzes the polymerization of the deoxyribonucleotides into a DNA strand. Taq polymerase, isolated from a bacterium called *Thermus aquaticus*, is one of the most commonly used since it can sustain the temperature required to denaturate DNA. DNA primers, typically synthetically produced

oligonucleotides, are used to produce a starting point for the synthesis. The chain reaction constists of three steps, the first of which is a denaturation step. In the step the buffer solution is heated up in order to denaturate the template. The denaturation is followed by an annealing step in which the solution is cooled down to let the primers attach to the 3' ends of the single strands of the denatured template. In the third step the polymerase synthesizes a new DNA strand complementary to the template strand by adding deoxynucleoside triphosphates, dNTPs. This happens by condensing the 5'-phosphate group of the dNTPs with the 3'-hydroxyl group at the end of the extending DNA strand (starting from the primer). The denaturation step requires typically temperature of 94 °C and one minute. The anneling happens typically at 55-65 °C (below the melting point of the primers) in one minute. Taq has its own optimum activity temperature around 72 °C. The elongation step takes usually 1-2 minutes, and about thousand bases are synthetized every minute. [9]

1.2   DNA conductivity

Already in the early 1960s it was proposed that DNA strands could serve as electrical wires due to the π-orbital overlapping of the base pair stack. It is the long-standing hope of many scientists that the unique properties of DNA could be further exploited in the design of electronic circuits. Charge transfer (CT) experiments in natural DNA in solution have shown high transfer rates [10], whereas electrical transport experiments carried out on DNA molecules have shown a variety of possible behaviors, i.e. insulating [11–24], wide-gap semiconducting [25–32], and ohmic (or nearly ohmic with a small activation gap) [33–45].

Experiments on single poly(GC) oligomers [43] in aqueous solution as well as on a single suspended DNA [25] with a more complex base sequence have shown relatively high currents. Thus DNA may conduct given the right environmental conditions. Up to date no highly conductive forms of DNA have been found, at least not conductive enough to be used as a building block as such.

1.2.1   Charge Transfer

CT through a DNA bridge has been studied [46,47] chemically by generating a donor, i.e. a radical cation (typically G+ because it has the lowest oxidation potential), and using a site consisting of three consecutive GC pairs as an acceptor with an ionization potential that is 0.7 eV lower than for a single GC pair. In the experiments

holes were found to migrate from the donor to the acceptor through a DNA bridge consisting only of AT pairs. [10] Other method to study CT is to use photoexcitations. For example, in the pioneer studies by Barton *et al.* [48, 49] ruthenium(II) and rhodium(III) were used as a donor and an acceptor, respectively. When two complementary oligonucleotides, one containing the donor and other the acceptor chemically bonded to the oligonucleotide, were hybridized so that the donor and the acceptor were at the different ends of the duplex, the steady-state luminescence of the ruthenium(II) was completely quenched. [7]

In this sort of experiments the simplest model is tunneling through a one-dimensional energybarrier for which the rate of tunneling reads

$$k_{\mathrm{CT}} = k_0 e^{-\beta R}, \tag{1.1}$$

where R is the distance between the acceptor and the donor and β is a constant describing how fast tunneling rate falls off as a function of the distance. In more detailed considerations sequential tunneling processes and thermally activated hopping are also considered. Barton's group pointed out that the rate of CT can vary from insulator-like (~ 1 Å^{-1}) to wire-like (~ 0.1 Å^{-1}) depending on energetics (donor, acceptor, base stack), the distance R, and base sequence and integrity of the stack. [7] Actually, it seems that the main factor causing contradicting results is the coupling of the donor and the acceptor to the DNA molecule [50].

There is a consensus that the G rich sites are responsible for the hole transfer due to their lower ionization energy, i.e. holes use sites rich in G as stepping stones between AT sites. As a conclusion, in the case of long DNA molecules which usually contain too large A-T bridges for a pure tunneling mechanism, efficiency of CT can not be described by parameter β anymore. In addition, in typical DC measurements the energies are too low for excited states, and consequently pure sequential tunneling, to occur in longer DNA molecules. [7]

1.2.2 Electronic conduction

Theoretical aspects

The electronic energetics of a double-stranded DNA chain should take into account contributions coming from the base stack, the backbone, and the environment. The resulting energy network can be arranged starting from the high energy values related to the on-site energies of the bases and sugar-phosphate groups (8-12 eV). Next are the energy values related to the hydrogen bonding between Watson-Crick

pairs ($\sim$0.5 eV) and the coupling between the bases and the sugar moiety ($\sim$1 eV). The aromatic base stacking deals with energies from 0.01 eV to 0.4 eV. It should be noted that the energy scale of the environmental effects (such as presence of counter ions and water interacting with the bases and the backbone by means of hydration, solvation, and CT processes) is about 1-5 eV. [10]

There are several theoretical approaches suitable for studying the transport in 1D DNA strands and they are usually based on the tight-binding model. Variation in the sequence of the base pairs almost forces one to use methods well-known from the theory of disordered systems. Effectiveness of the electronic transport is usually characterized by localization length, which describes whether an electron can move along the DNA or not. The vast majority of the studies agree that the transport properties upon including some degree of energetic disorder tend towards insulating side. [10]

In the aromatic rings of the bases (figure 1.2), the atomic orbitals perpendicular to the plane of the ring form delocalized π bonding and π^* antibonding orbitals. If electronic coupling between π orbitals of adjacent base pairs is strong enough, the energy level broadening reduces the energy gap between π and π^* states (about 4 eV), which could lead to ohmic or semiconducting behavior. [51]

Anisotropy

Okahata *et al.* observed [29,30] anisotropic conductivity in aligned DNA cast films. It took until late '90s before the first measurements on single DNA molecules could be realized, which was mainly due to the fact that nanofabrication methods were less advanced at that time. Measuring on single molecules allows one to measure the conductivity along DNA since the molecule can be precisely immobilized to the desired position. [7]

Earlier measurements

Electrical measuments on DNA films, molecules, and bundles have shown very contradicting results. This is the case since it is very hard to obtain reproducible and reliable results from the experiments with nanoscale molecules. First of all, the contacts between the electrodes and the DNA molecule(s) should be ohmic and low in resistance to avoid extra nonlinearities and to make sure that the resistance measured is that of the molecule(s). Secondly, environment is a crucial factor, and it should be orders of magnitude more insulating than the molecule. [52]

In addition, things such as water, ions, topology, and possible charge of the surface on which the molecule is lying might modify the electronic conductivity through conformation distortions, mechanical stress, or net charge affecting the possible conduction channel. Base sequence of the molecule can also be important since a very non-periodic sequence might cause the orbitals, i.e. the possible conduction channel, to lose their overlap. Although, a very periodic sequence is not good either because it is bad for the hybridization. Last but not least, one cannot image or probe a nanoscale system without disturbing it somehow. For example, imaging the structures by atomic force microscopy (AFM) might dope the DNA strands. [10,53]

1.3 DNA structures

DNA nanotechnology is based on the self-assembly (SA) properties of DNA. SA is a process in which building blocks form an ordered structure. The process is driven by the general principle of minimizing the internal energy and is usually based on the weak interactions, e.g. van der Waals, capillary, π–π bonding, and hydrogen bonding. The key point is that the building blocks can be anything, e.g. atoms, molecules, small, or even mesoscopic structures. This section is about DNA structures which have been fabricated using methods based on SA. The methods currently developed rely on mainly two approaches: tiles and the origami method. Both methods have been succesfully used to create 2D and 3D DNA structures, such as lattices, nanotubes, cubes, octahedra, tetrahedra, and polyhedra. [53]

1.3.1 Sticky ends, Holliday junction, tiles

The so-called "sticky ends" are short ssDNA overhangs at the end of dsDNA molecules. If two dsDNA molecules have complementary sticky ends, the molecules can combine by base-pairing, which leads to 1D constructs. In order to create more complex structures Seeman *et al.* introduced branched DNA molecules which are formed of three to eight ssDNA molecules linked together through a common crossover point. [55] The branched junction (figure 1.4) formed of four double-helical arms, i.e. eight ssDNA molecules, is analogous to the Holliday junction which appears in nature during meiosis. During meiosis the branch point is able to migrate, which is not a good thing considering creation of stiff structures. Seeman *et al.* found a way around this by carefully designing the base sequence so that the branch point remains immobile [56]. The branched DNA molecules with immobile branch points
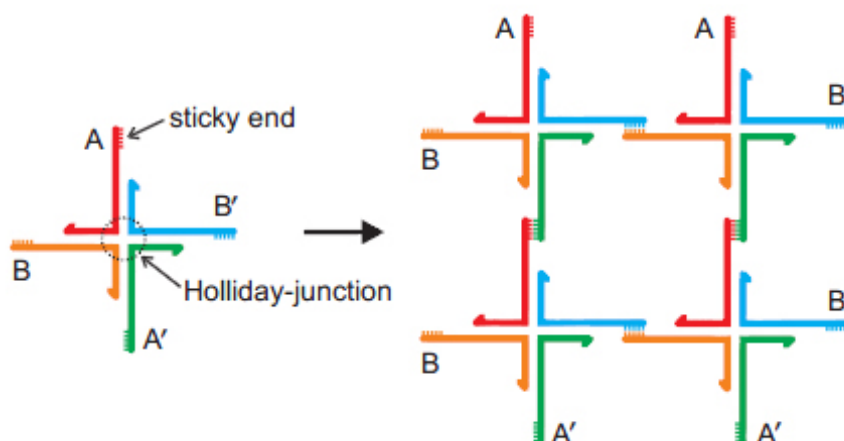
Figure 1.4: *The branched DNA molecule with four double-helical arms analogous with Holliday junction and the idea how sticky end hybridization leads to a 2D lattice. Sticky ends A, B are complementary to A', B' respectively. The image is adapted from [54].*

can be linked together through hybridization of sticky ends thus allowing building of 2D constructs.

Individual branched junctions as such were too flexible to form rigid larger 2D arrays. The first attempts to create more rigid structures involved DNA structures containing two or three dsDNA helices lying in a plane linked by strand exchange at two or four immobile crossover points. These structures are called double crossover (DX) and triple crossover (TX) molecules. [57, 61, 63] There are several types of DX and TX crossover molecules, differentiated by the relative orientations (parallel or antiparallel) of their helix axes, the number of double helical half-turns (even or odd) between crossovers, and the possible DNA hairpins added. Since then, many different kinds of crossover molecules, or "tiles", have been introduced thus producing a large variety of diverse 2D arrays. Figure 1.5 shows two types of DX tiles, DAE and DAO, and ways to produce two different lattices using them, and figure 1.6 shows various experimentally tested tiles.

The tile approach has some serious limitations: First of all, DNA sequences for tiles should be carefully designed to avoid secondary structures and unwanted interactions, and because the size and shape of the produced lattices are very hard to control. Secondly, the synthesis involves interactions between a large number of short oligonucleotides, and thus the yield of complete structures is highly sensitive to stoichiometry (the relative ratios of strands). The synthesis of relatively complex structures requires multiple reaction steps and purifications and, in the end, the yield
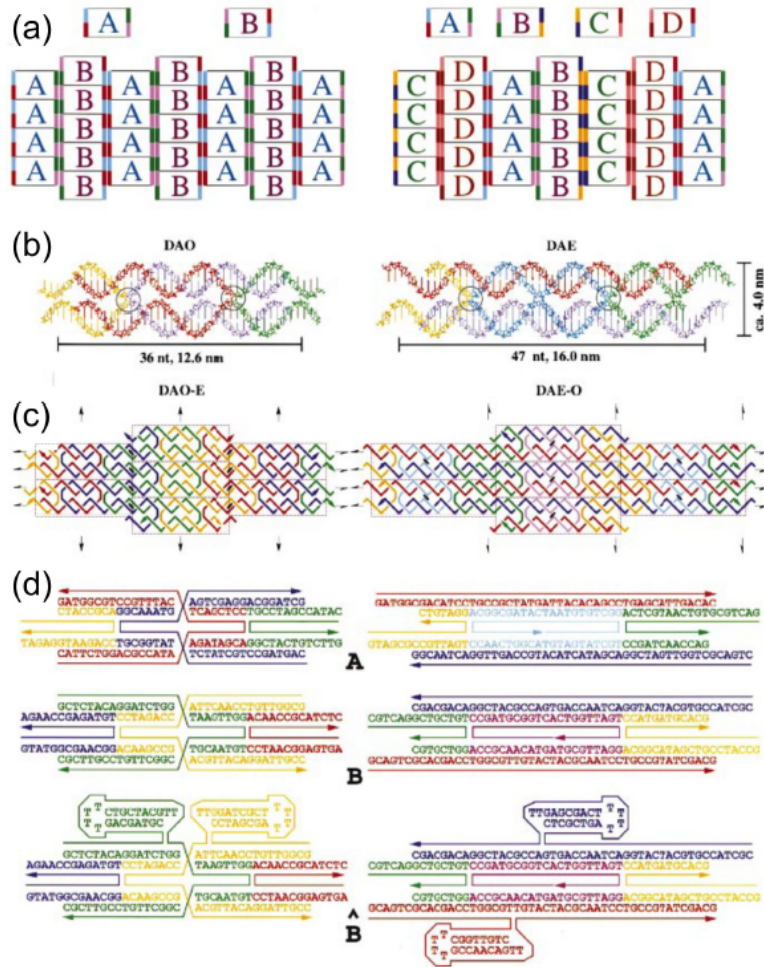
Figure 1.5: *a) The logical arrangements of two different DX lattices, DAO-E (left) and DAE-O (right), consisting of four different DX tiles. Each tile contains sticky ends which have to match with the ends of the adjacent tiles. b) Models of single DAO (DX, antiparallel, odd spacing) and DAE (DX, antiparallel, even spacing) tiles. Each strand is shown in a unique color and crossover points are circled. c) The produced lattice topologies, where each DX unit is highlighted by a rectangle. A unique color is chosen for each different type of strand which would be formed after covalent ligation of the assembled tiles. DAO-E design produces four distinct strand types, each continuing infinitely in the vertical direction, whereas DAE-O design contains two small circular strands and four infinite strands, two of which extend horizontally and two of which extend vertically. d) The actual oligonucleotide sequences used. The tile $\hat{B}$ is a version of B containing additional DNA hairpin sequences, which serve as topographical labels for AFM imaging, showing increased height. The image is adapted from [57].*
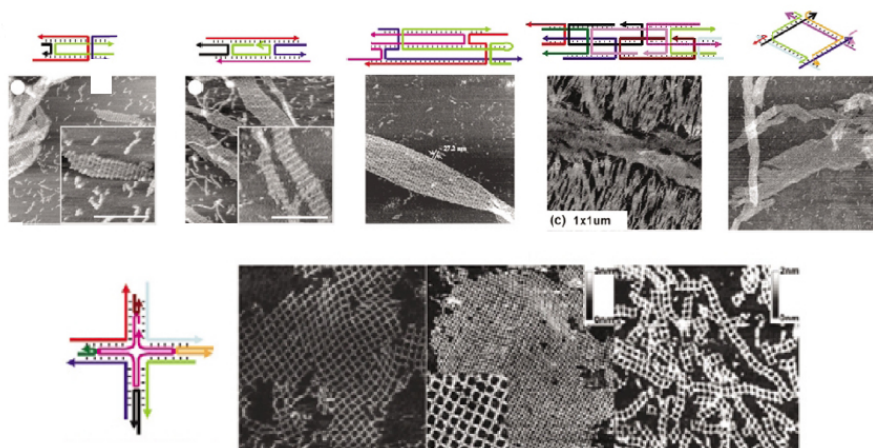
Figure 1.6: *Schematic structures of experimentally tested tile structures and AFM images taken of the ready lattices. The images are adapted from [57–62].*

might still be low. [53]

1.3.2 The origami method

Paul Rothemund came up with an alternative approach to creating 2D DNA structures [64]. Instead of tiles it is based on folding a linear DNA scaffold, i.e. a 7.3 kb single-stranded viral genome, into a desired shape. The folding is done via short nucleotides, so-called staple strands. Designing a structure is relatively easy compared to the tile approach and the structures can be almost arbitrary. A schematic picture of an origami structure and some ready structures are shown in figure 1.7. The synthesis happens in one step, relative consentrations of the staple strands do not matter, even the absolute consentrations do not have to be exact, and the yield is usually high.

1.3.3 DNA structure as a breadbroad

Oligonucleotides, and DNA in general, can be modified to contain functional groups which can serve as binding sites for other molecules. Therefore, it is possible to use DNA and/or DNA structures as templates for assembly of other materials.

Linear DNA has been metallized to form a nanowire [65]. Furthermore, both linear DNA and 2D structures have been used as templates for e.g. semiconducting nanoparticles (lattice [66]), metal nanoparticles (linear [67] and lattice [68–71]), CNTs (linear [72] and lattice [73]), and proteins (linear [74] and lattice [59,62]). DNA
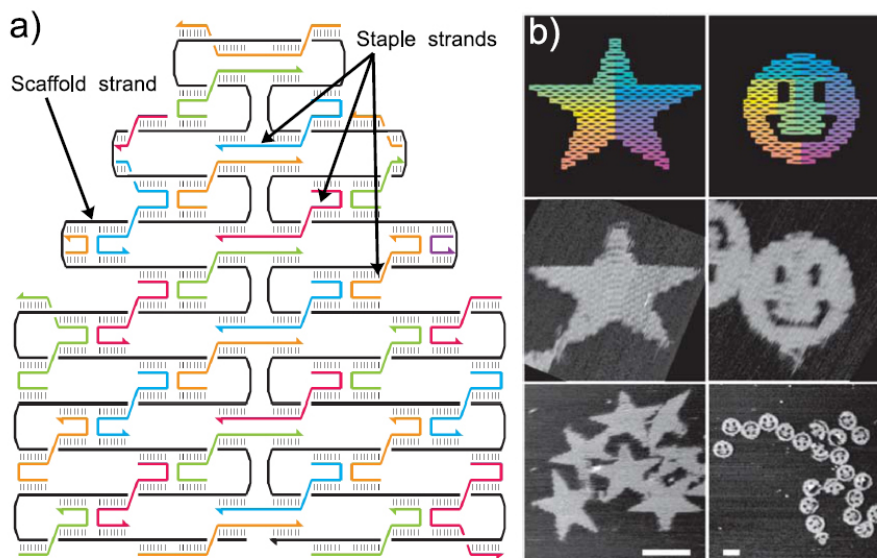
Figure 1.7: *a) A schematic picture of an origami structure b) Examples of origami structures. The image is adapted from [64].*

templates could allow fabrication of large patterned structures with a resolution comparable to current lithography techniques.

2D structures built via tiles approach are typically periodic and thus non-periodic assembly is rather difficult. Furthermore, assembly of multiple materials requires multiple attachment chemistries since the materials are assembled on prefabricated DNA templates. [53]

The origami method on the other hand does not suffer from the limitations discussed above. Each staple strand has it is unique position on the structure and can be modified separately, thus the name breadboard. The resolution is determined completely by the staple strands and the size of the formed structure by the length of the scaffold. So far origami method has been applied to arrange e.g. proteins [75,76], gold nanoparticles [77], and CNTs [73].

1.4 Dielectrophoresis

1.4.1 Theory of dielectrophoresis

Dielectrophoresis (DEP) is a phenomenon in which a particle feels a net force caused by a nonuniform electric field. The principle of DEP is shown schematically in figure 1.8. In a uniform field the net force due to the Coulomb interaction is zero because

the polarized surface charges cause an electric field opposite to the original electric field. However, in a nonuniform field there is a left-over net force. This simplified model does not take into account the polarization of the medium, but in a general case it should also be taken into account. Due to this DEP can be either positive or negative the former occuring when the matter has a higher polizability than the medium. The matter is in that case pushed towards the region of higher electric field. In the case of negative DEP the situation is vice versa. [7]
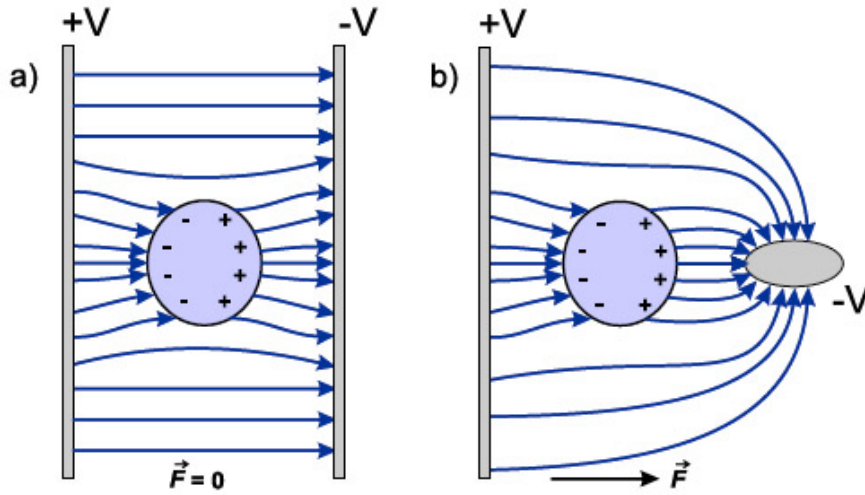

Figure 1.8: *a) uniform electric field, net force is zero b) nonuniform electric field, net force drives the particle to the region of higher electric field, positive DEP.*

The simplest approach to estimate the resulting force is to look at the effective dipole moment caused by the particle and the medium. The dipole moment is proportional to the electric field as

$$\vec{p} = \alpha\vec{E} = 3V\epsilon_{\mathrm{m}}\Re[K]\vec{E}, \tag{1.2}$$

where V is the volume of the particle, α polarizability, ϵ_{m} permittivity of the medium, and K the Clausius-Mossotti factor which depends on both the particle and the medium as

$$K = \frac{1}{3}\frac{\epsilon_{\mathrm{p}}^* - \epsilon_{\mathrm{m}}^*}{\epsilon_{\mathrm{m}}^* - A(\epsilon_{\mathrm{p}}^* - \epsilon_{\mathrm{m}}^*)}. \tag{1.3}$$

A is a geometrical factor which varies from $1/3$ (sphere) to 1 (short rod) and ϵ_{p}^*, ϵ_{m}^* are complex permittivities of the particle and the medium, respectively, given by

$$\epsilon_{\mathrm{p}}^* = \epsilon_{\mathrm{p}} - j\frac{\sigma_{\mathrm{p}}}{\omega} \tag{1.4}$$

$$\epsilon_{\mathrm{m}}^* = \epsilon_{\mathrm{m}} - j\frac{\sigma_{\mathrm{m}}}{\omega} \tag{1.5}$$

in which ω is the angular frequency of the electric field and σ_{p}, σ_{m} the conductivities of the particle and the medium. The net force acting on a small dipole can be written as

$$\vec{F} = (\vec{p} \cdot \nabla)\vec{E}, \tag{1.6}$$

where $\vec{p}$ is the induced dipole moment and $\vec{E}$ the electric field. By combining equations (1.2) and (1.6) one obtains the so-called DEP force

$$\vec{F}_{\mathrm{DEP}} = \frac{1}{2}\alpha\nabla(E^2), \tag{1.7}$$

from which one can easily see that the direction of the force does not depend on the direction of the electric field. Instead, it follows the sign of the Clausius-Mossotti factor (positive versus negative DEP) which is dependent on the applied frequency. Furthermore, the magnitude of the force is largely dependent on the gradient. [7]

It should be noted that the DEP force depends on the volume of the particle, which is a limiting factor when manipulating nanoscale particles. This is due to the fact that the particle must also overcome the Brownian motion which is roughly given by

$$F_{\mathrm{Brownian}} = \frac{k_{\mathrm{B}}T}{V^{\frac{1}{3}}}, \tag{1.8}$$

where k_{B} is the Boltzmann constant and T temperature. Thus very large gradients are typically required. The equation of the DEP force (1.7) was derived classically, which means that it does not take into account all things involved. Most of the atoms of a nanoscale particle usually reside on the surface and a counter-ion cloud typically forms if the particle happens to be charged. Furthermore, several things, like AC electro-osmosis and Joule heating which cause flow of a liquid medium, can make the situation more complicated [78].

1.4.2 Dielectrophoresis and immobilization of DNA

First success in DEP studies of DNA was in the '90s when Washizu *et al.* managed to trap λ-DNA between electrodes with a separation of 60 μm so that the molecules aligned along the electric field [79, 80]. Later on, they measured the fluorescence of pUC18 plasmids under a stationary AC field [81]. Mainly, they studied the dependence of the polarization on the frequency and intensity of the field. The polarizability of the DNA plasmids was several orders of magnitude larger than that of a conducting ellipsoid with the same dimensions. This implied that DNA in a buffer solution is larger in an electrical sense because of the counterion cloud that

forms around the DNA molecule. They also noticed that increasing pH of the buffer increased the polarizability.

Since then, there have been many studies on DEP of DNA with different aims, e.g. positive versus negative DEP [82, 83], stretching of DNA [80, 84], trapping efficiency [85, 86], measuring the polarizability [85, 87], and electrodeless trapping [88]. In other words, many studies have aimed to create methods to separate DNA fragments or immobilize them to a certain location for further use by using DEP. From the viewpoint of measuring the conductivity of DNA, interesting is that in 2003 Hartzell *et al.* trapped and immobilized [34, 35] λ-DNA between gold electrodes with 8 μm spacing using thiol-groups, after which they measured the conductivity. This approach was used later by Tuukkanen *et al.* at NSC [85].
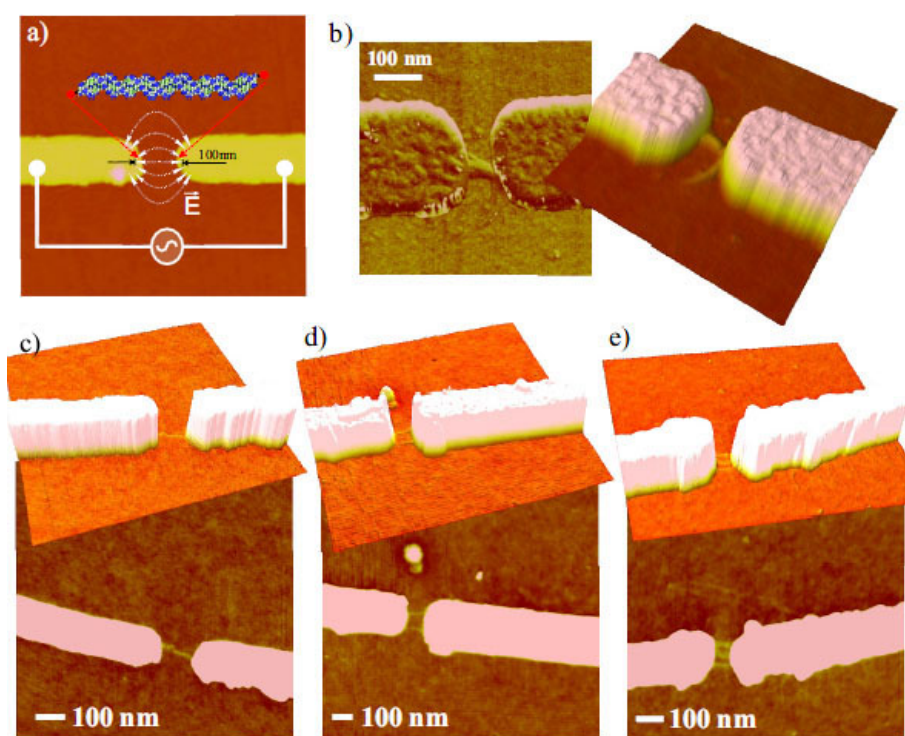
Figure 1.9: *a) A schematic picture about the DEP of DNA with finger-tip type electrodes b) An AFM image of a trapped DNA bundle c)-e) One, two and three individual trapped DNA strands. The image is adapted from [85].*

As one can see from equation (1.7), the DEP force can be increased by either increasing the strength or the gradient of the electric field. However, too high fields can induce harmful fluid flows, heating, and even electrolysis. To avoid this problem, Tuukkanen *et al.* used very narrow fingertip type gold electrodes [85] (figure 1.9) and CNTs [89] as electrodes to create high field gradients. It was shown that the amount

of DNA labeled with fluorescent molecules, i.e. intensity of fluorescence in the gap between the electrodes, increased with voltage, V, after a certain minimum voltage, $V_{\min}$, as

$$I = I_0 + A(V_{\min}^b + V^b)^{2/b}, \tag{1.9}$$

where I_0, A are fitting constants. The parameter b determines the rate of the asymptotic change from a constant value, i.e. $I_0 + AV_{\min}^2$ which is very small, to V^2 dependency. The best fit to the data was found using the value $b = 40$.

The minimum voltage occurs when the time-average of the DEP potential equals the thermal energy associated with the Brownian motion (i.e. the Brownian motion does not overcome the potential well caused by the DEP):

$$U_{\text{DEP}} = -\frac{1}{2}\alpha E^2 = -\frac{3}{2}k_{\text{B}}T = -U_{\text{Thermal}}. \tag{1.10}$$

Computer simulations on the electric field produced by the electrodes and the known minimum trapping voltage were used to calculate the polarizability (α) per bp for the used DNA fragments (27-8,461 bp) [89, 90]. It was discovered that the polarizability was higher for the the short molecules, which agrees with the relative size compared to the counterion cloud. Using higher frequencies (1-10 MHz) for trapping required high voltages, which can be explained by the time-scale of the polarization, whereas with lower frequencies (0.1-1 MHz) the trapping was most efficient. However, with higher frequencies the molecules were better localized between the electrodes, which can be explained by decreased spreading of the DNA spot [88] due to thermal and electro-osmotic flows. The optimal frequency was found to be about 1 MHz.
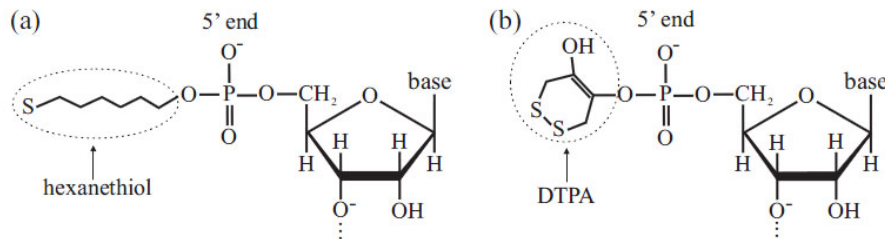

Figure 1.10: *a) hexanethiol (C6-thiol) b) dithiol-phosphoramidite (DPTA) at the 5'-end of an oligonucleotide.*

The immobilization of DNA on the gold electrodes through sulphur-gold bonding was also studied by Tuukkanen *et al.* Two different modifications on oligonucleotides of essentially the same length (figure 1.10) were used: hexanethiol (C6-thiol) and

dithiol-phosphoramidite (DTPA). The quantitative analysis was done by comparing the amount of fluorescence remaining after turning off the DEP voltage. As expected, the molecules without a linker diffused away quickly. It was found out that the C6-thiol linker bound more efficiently compared to the DPTA, which was not expected since DPTA has 2 sulphur atoms, whereas C6-thiol only has one. [90] Density functional theory (DFT) calculations were performed (see reference [91]) for better understanding of the binding process. The calculations showed that the C6-thiol can bind to a tetrahedral gold atom cluster of 20 atoms with a binding energy of 1.8 eV, whereas the DPTA linker did not show any binding affinity if the S-S bond was left intact. However, partial hydration of S-S bond resulted in binding with an energy of 1.2 eV.

1.5 Impedance spectroscopy

In general, impedance spectroscopy (IS) is about studying electronic properties of any material, liquid or solid, and interfaces formed by these materials using electrodes. One can use it to study the dynamics of either free or bound charge inside a medium, close to the interface, or both. IS is divided into two categories: electrochemical IS (EIS) and everything else. EIS involves materials in which ionic conduction strongly predominates. Examples of such materials are electrolytes, fused salts, ionically conducting glasses and polymers, and nonstoichiometric ionically bonded single crystals. [92] EIS is also valuable in the study of fuel cells, rechargeable batteries, corrosion, and nowadays especially solar cells [93–95]. Electrochemistry is not involved when dielectric materials are in question, i.e. solid or liquid nonconductors, or materials with predominantly electronic conduction. Examples are single-crystal or amorphous semiconductors, glasses, and polymers. Of course, IS applies to more complicated situations as well, e.g. to partly conducting dielectric materials with some simultaneous ionic and electronic conductivity. [96] This section mainly focuses on AC-IS with no bias voltage applied, or there is only one bias voltage used at a time. There also exists a more sophisticated method called potentiodynamic EIS which is used to record impedance spectra as a function of both frequency and bias voltage [97].

It should be noted that most of the methods and theory involving EIS have been developed for macroscopic and mesoscopic systems. However, in this thesis EIS has been used to characterize a system in nanoscale.

1.5.1 Impedance as a complex quantity

In a typical impedance measurement the electrochemical system is perturbed by an electrical stimulus and the response monitored as a function of the perturbation frequency. Let us assume a monochromatic perturbation signal, now an alternating voltage

$$v(t) = V \sin(\omega t), \tag{1.11}$$

is fed into the system, and an alternating current is obtained as a response:

$$i(t) = I \sin(\omega t + \theta). \tag{1.12}$$

V, I are amplitudes, ω is angular frequency, t time, and θ phase difference. In time domain the relationship between the perturbation and the response involves a (possibly very large) set of differential equations. This problem is removed provided that the system fills the following criteria [98]:

- **Causality:** The response of the system is completely determined by the perturbation.

- **Linearity:** All the differential equations describing the system must be linear.

- **Stability:** The system must return to its original state when the perturbation is turned off.

Both the perturbation (1.11) and the response (1.12) can be Fourier transformed into frequency domain. Provided the above conditions a linear relationship between the two is found:

$$\mathcal{F}\{v(t)\} = V(j\omega) = Z(j\omega, I)I(j\omega) = Z(j\omega, I)\mathcal{F}\{i(t)\}. \tag{1.13}$$

$\mathcal{F}\{\}$ is the Fourier transform, $V()$ and $I()$ are the transformed voltage and current, j the imaginary unit, and $Z()$ the impedance, i.e. the transfer function between the perturbation and the response. In general, current could be used as a perturbation also as long as the linearity holds. [92]

Most of elecrochemical systems are highly nonlinear, i.e. each used perturbation frequency generates harmonic response frequencies. However, by using small perturbation amplitudes the system can be described via a small-signal model. The used amplitude should be of the order (preferably smaller) of the thermal voltage, $V_{\mathrm{T}} = kT/e \approx 26$ mV in room temperature (k is Boltzmann constant, T absolute temperature, e elementary charge). [92]

As a complex quantity impedance can be presented in the following forms:

$$Z(\omega) = |Z(\omega)|e^{j\theta(\omega)} = |Z(\omega)|(\cos(\theta(\omega)) + j\sin(\theta(\omega))) = Z'(\omega) + jZ''(\omega), \quad (1.14)$$

where $|Z|$ is the magnitude, $\theta = \tan(Z''/Z')$ the phase difference between the voltage and the current, Z' the resistance (real part), and Z'' the reactance (imaginary part). The inverse of the impedance is called an admittance.

1.5.2 Electrode systems

The simplest EIS setup has two electrodes. It is assumed that the potential drops linearly between the electrodes generating a uniform electric field. This is not the whole truth since there exists a polarization layer or a double layer (DL) formed by ions on both electrodes generating a potential drop. Nevertheless, if the effects of the electrode-medium interface (i.e. the potential drop because of a layer and/or a bad contact) are not significant, the method is very usable to obtain information about the overall impedance of the system. This is often the case when dealing with dielectrics with no electrochemistry involved. [96]

Since the bulk properties, such as resistance and capacitance, are typically extensive quantities and do not always govern impedance spectra, it is essential what happens at the electrodes. In an electrolytic cell the static space-charge fields are absent only when charge at the working electrode is zero. This can be archieved by using a small working electrode, a very large counter electrode, an inert very small reference electrode with a known potential, and by adjusting the external static voltage so that the point of zero charge (PZC) is obtained at the working electrode. In general, the current distribution near the working electrode depends on frequency and has a contribution to the overall impedance of the system, but the kinetics depend strongly on the external applied voltage. This method is typically used when dealing with EIS. [96]

If one wants to eliminate effects caused by the electrode reactions, one must use a system of four electrodes. The two end electrodes serve as in the case of two electrodes, i.e. generate the potential drop and thus a current. What is different, is that the two electrodes in between are used to measure voltage and have a very high input impedance, which causes no current to flow through them. In this case, the electrical parameters of the material portion between the voltage electrodes can be evaluated without interface polarization because all the current flows through the end electrodes. [99–101]

Besides the electrode-material interface there might exist other interfaces in the bulk region. The medium is not always completely homogeneous, i.e. there might be crystal boundaries (Frenkel layers) and local changes in concentration that cause static fields. These interfaces also show up in an impedance spectrum, typically as parallel RC circuits with a characteristic time constant. [92]

1.5.3   Double layer, electrolytes

The double layer (DL) formed on an electrode is often described by the Gouy-Chapman model which takes into account the combined effects of electrostatic forces and thermal motion giving a rise to a diffuse layer of excess ions. The layer consists essentially of two regions: the Stern layer (SL) and the diffuse layer. The SL further divides into two segments: the inner and outer Helmholtz plane (IHP and OHP). [102] The ions in the electrolyte are divided into two categories: chemically specifically adsorbed ions and indifferent ions. The former form the IHP and determine the surface charge of the electrode, whereas the latter occupy the OHP. The ions in the OHP feel (in this model) only the Coulombic forces, screen the surface charge, and yet participate in the thermal motion (somewhat free to move). [102,103] Because of this screening, there exists always some capacitance which can be described as a DL capacitance (dlc). The model is further clarified in the figure 1.11. Tangential stress can move the diffuse layer, or at least part of it. The plane that separates mobile fluid from the attached fluid is called a slipping plane.

The electric potential between the bulk electrolyte and the SL is called a Stern potential, whereas the potential between the bulk and the electrode/particle surface is called an electric surface potential. In colloidal chemistry one uses a Zeta potential (ZP) to describe DLs. It is the potential between the bulk and the slipping plane of the DL around the solvated particle. The Stern potential and the ZP are not the same in general [104], but typically quite close to each other. The ZP is the only way to get information about the properties of the DL. It can be measured using electrophoresis, electroacoustic phenomena, streaming potential, and electroosmotic flow. A high ZP (about 50-100 mV for particles, but can be several volts on electrodes [104]) ensures high repulsion between adjacent similarly charged species, which prevents aggregation. Colloids with a lower ZP tend to coagulate or flocculate. The chemical composition of the sample at which the ZP is zero is called the PZC, which is typically determined by measuring the pH [isoelectric point (iep) in general]. This is due to the fact that protons and hydroxyl ions are the most
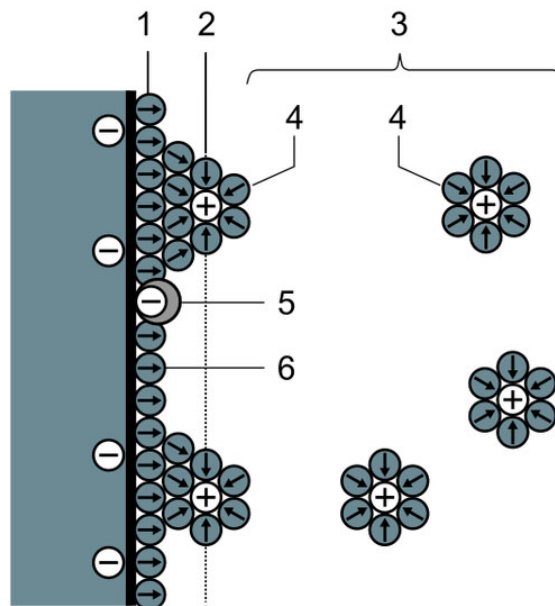
Figure 1.11: *1. Inner Helmholtz Layer, 2. Outer Helmholtz Layer, 3. Diffuse layer, 4. Solvated ions, 5. Peculiar adsorptive ions, 6. Solvent molecule.*

common charge-determining ions for most surfaces/particles [104].

The characteristic thickness of a DL is the Debye length. In aqueous solutions it is typically on the scale of few nanometers and the thickness decreases with increasing concentration of the electrolyte. In an electrolyte or colloidal dispersion the Debye length is given by [105]:

$$\kappa^{-1} = \sqrt{\frac{\epsilon_r \epsilon_0 k_B T}{2 N_A e^2 I}}, \tag{1.15}$$

where ϵ_r is the dielectric constant, ϵ_0 permittivity of free space, N_A Avogadro number, and I is ionic strength. The ionic strength in turn is given by [106]

$$I = \frac{1}{2} \sum_{i=1}^{n} c_i z_i^2, \tag{1.16}$$

where c_i is the concentration (mol·dm^{-3}) and z_i is the charge of ion i.

In EIS an important distinction is made between supported and unsupported electrolytes. The former contains a high concentration of indifferent electrolyte, i.e. ions that generally neither adsorb nor react at the electrodes. This ensures that the material is almost electroneutral everywhere, thus allowing diffusion and reaction effects for the low-concentration ion of interest to dominate the AC response. Generally, support is only possible for liquid electrochemical materials, and

thus solid electrolytes are unsupported in most cases of interest. In unsupported conditions electroneutrality is not present, and Poisson's equation strongly couples charged species. Because of this difference, the formulas or models used to analyze supported and unsupported situations may be somewhat different, even completely distinctive. [96]

1.5.4 Equivalent model

The data obtained by AC-IS is 3D (four-dimensional in potentiodynamic EIS), i.e. the data spans a discrete 3D set (ω, Z', Z'') or $(\omega, |Z|, \theta)$. The data can be presented by using 3D graphs, but more common is to use multiple 2D presentations, e.g. Bode and Cole-Cole plots. Amplitude, $|Z|$, and phase, θ, plots with a logarithmic frequency scale are called Bode plots (although gain, in decibels, versus logarithmic frequency plots are also called Bode plots). The Cole-Cole plots are of the form $(Z', -Z'')$. An equivalent model is a theoretical model into which the measured data can be fitted by using the CNLS method (Complex Nonlinear Least Squares). The equivalent circuits consist of the ideal elements and special frequency dependent distributed elements.

The biggest challenge with equivalent models is the physical interpretation. Both intuition and theory should be used when designing the model. The fact that the same data can be fitted into multiple differently organized circuits produces even more challenge. This problem can be overcome by varying the conditions/parameters of the system, e.g. applied bias voltage, pH, concentrations, and temperature. [92]

An ideal resistor is usually used to describe energy losses in a system, e.g. Ohmic losses in the bulk or losses due to reaction and adsorption processes at the electrodes. Capacitors and inductors usually describe processes which involve storing energy, e.g. transition currents because of geometrical capacitance or dlc. Electrode processes and interfaces are usually described by a parallel combinations of resistors and capacitors. This would yield a single time constant, $\tau = RC$ (R is resistance, C capacitance) per electrode process or interface. Unfortunately, the situation is not usually that ideal, and therefore lumped elements can seldom describe the whole system. In reality systems are highly nonideal, i.e. quantities depend on geometrical factors (e.g. surface roughness) and distributions of microscopic properties (e.g. local concentration changes and adsorbed impurities). Furthermore, nonlocal diffusion processes should also be taken into account. [92]

Faradic Charge Transfer Resistance

The charge transfer (CT) resistance (ctr) arises from the general Butler-Volmer equation, which describes the Faradic current produced by an electrode (both cathodic and anodic reaction occur on the same electrode):

$$i = A i_0 \left[\frac{C_o(0,t)}{C_o^*} \exp\left(\frac{(1-\beta)nF}{RT}\eta \right) - \frac{C_r(0,t)}{C_r^*} \exp\left(-\frac{\beta nF}{RT}\eta \right) \right], \qquad (1.17)$$

where A is the active surface area, i_0 the exchange current density, $C_o(0,t)$ and $C_r(0,t)$ the time-dependent concentrations of the oxidized and reduced species at the electrode surfaces, C_o^* and C_r^* the same in the bulk electrolyte, n number of electrons involed in the reaction, F Faraday constant, R universal gas constant, η the overpotential (difference from the equilibrium potential), and β a dimensionless symmetry factor. At low overpotentials the above equation simplifies to

$$i \approx A i_0 \frac{nF}{RT}\eta \qquad (1.18)$$

if the concentrations at the electrode are about the same as in the bulk. In that case the ctr (for one electrode) is given roughly by

$$R_{ct} = \frac{1}{\partial i/\partial \eta} \approx \frac{RT}{nFAi_0}. \qquad (1.19)$$

[107] The ctr is usually used in supported situations in combination with dlc to describe a system with fast electrode reaction(s).

Constant Phase Element

As mentioned earlier, the capacitors can seldom describe the whole microscopic behavior of a system. Instead, the capacitor is usually replaced by a distributed element called constant phase element (CPE) of the form:

$$Z_{CPE} = A(j\omega)^{-\gamma}, \qquad (1.20)$$

where A and γ are constants so that $-1 \leq \gamma \leq 1$, which means that the CPE can present any of the ideal elements or something between them. The CPE arises from a distribution of time constants. [92] The parameter γ is often used as a qualitive measure for surface roughness of a given microscopic system, but it can also arise from a distribution of electrochemical activation energies [108], chemical inhomogeneities [109], or nonuniform currents [110].

Figure 1.12 shows a typical response by a parallel combination of a CPE and a resistor, and the usual response of an RC circuit for comparison.
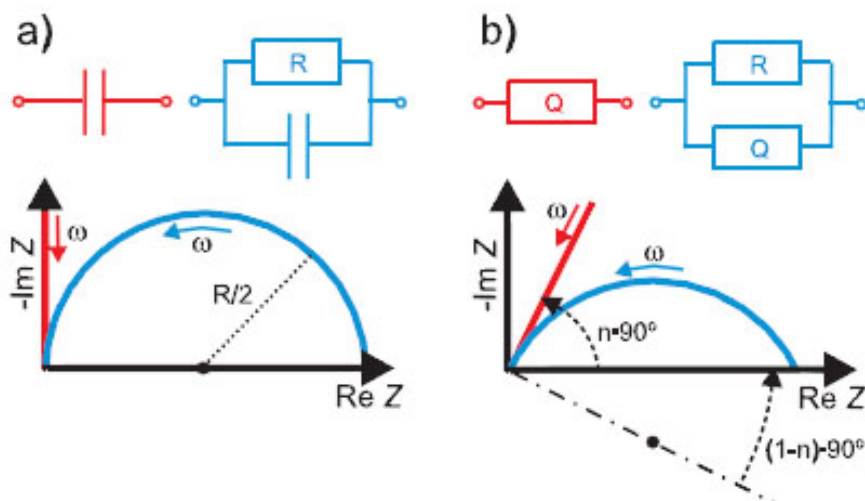
Figure 1.12: **a)** *A schematic $(Z', -Z'')$ plot of a plain capacitor (straight line) and a parallel combination of a resistor and a capacitor (semicircle with a radius of R/2).* **b)** *The impedance spectra change when a capacitor is replaced with a CPE. The response produced by a single CPE is a straight line at an angle of $n \cdot 90^\circ$ with respect to the Z' axis [n is the exponent of the CPE, see (1.20)]. A combination of a CPE and a resistor in parallel forms a semicircle, with the center lying on the axis tilted $(1-n) \cdot 90^\circ$ with respect to the Z' axis. Arrows indicate the direction of increasing frequency.*

Diffusion

The first distributed element derived was the Warburg diffusion impedance of semi-infinite range which can be derived from Fick's second law (i.e. continuity equation combined with Fick's first law) in 1D:

$$Z_{\mathrm{W}} = \frac{B}{\sqrt{j\omega}}, \tag{1.21}$$

where B is a constant. The model assumes electroneutrality, i.e. unrestricted diffusion in the bulk, and kinetically reversible electrodes. Electrodes are said to be kinetically reversible when the rate of the CT is not limited by the electrode reaction, i.e. it is only necessary to take into account the mass transport.

Other models for the same conditions also exist. For example, the Warburg impedance of short range which involves continuous diffusion and reaction, i.e. the Faradic current does not decay:

$$Z_{\mathrm{Wc}} = \frac{C}{\sqrt{j\omega}} \tanh\left(D\sqrt{j\omega}\right), \tag{1.22}$$

where C and D are constants. The condition is met usually by having high enough concentration of the active species and using a rotating disk electrode which keeps the bulk concentration homogeneous. This is especially important when one uses high bias voltages (overvoltages). [92] This kind of situation corresponds to adsorbing boundary conditions at the eletrode surface [111].

Another model involves short range diffusion and a fixed amount of the active species, which means that the diffusion from the bulk to the electrode will eventually stop, i.e. the diffusion gets blocked:

$$Z_{\text{Wn}} = \frac{G}{\sqrt{j\omega}} \coth\left(H\sqrt{j\omega}\right), \tag{1.23}$$

where G and H are constants. [92] This situation in turn corresponds to reflecting boundary conditions at the eletrode surface [111].

The equation (1.22) applies also to unsupported univalent short-range conditions as long as electroneutrality of the bulk can be assumed. In addition, it also holds when the electrode separation becomes comparable to the Debye length. Although, in that scale the condition of electroneutrality seldom holds. [112] Appearence of the Warburg impedance in a general unsupported case can be attributed to the action of the more mobile or more-reactive species in screening the applied electric field, allowing diffusion to dominate the motion of the remaining species. [113]

The diffusion impedances presented above are derived for parallel plate electrodes, and thus do not take into account the effects of geometry. Results exist at least for cylindrical and spherical geometries in unrestricted and restricted conditions [the conditions of equations (1.22) and (1.23), respectively]. For further information, see e.g. [114].

Often one finds diffusive-like behavior with some other power of frequency than minus half [111]. It is common to use CPEs in those cases. CPE has no extensive behavior at low/high frequencies, and thus it is not physically realistic, but it can be used to describe the system over a certain frequency range. [92]

It should be noted that the diffusion impedances are typically in series with faradic resistances describing losses in the system. This is the case even in very careful considerations derived from a system of Nerst-Planck equations and continuity equations, taking into account Maxwell's displacement currents [112]. Typically the charging of the DL and the faradic effects are assumed non-coupled when in reality, especially with unsupported electrolytes or slow electrode reactions, this could be far from reality [92].

Example models

One of the most famous equivalent models is the Randles circuit (figure 1.13). It is response in the $(Z', -Z'')$ plane constists of a semicircle and a tail at the low frequency end that has a 45 degree angle. The solution resistance, R_s, causes a small offset, the parallel combination of the ctr, R_{ct}, and the dlc, C_{dl}, produces the semicircle, and the semi-infinite Warburg impedance, Z_W, is responsible for the tail. The model is typically used with supported systems in which the diffusion of the reactive species to the electrode is not hindered.
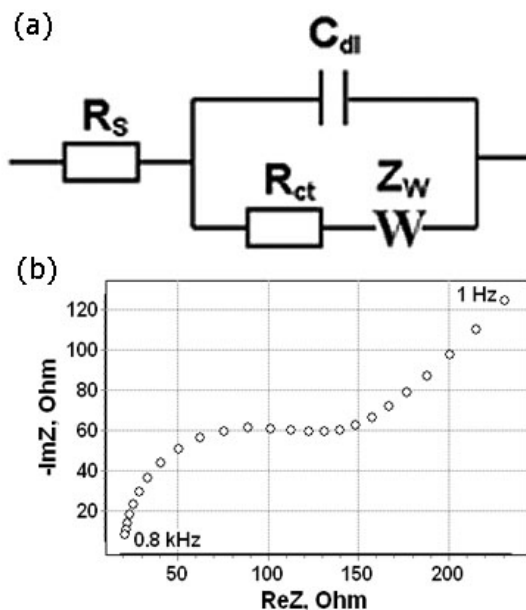

Figure 1.13: *a)* *The Randles circuit:* R_s *is the solution resistance,* R_{ct} *the ctr,* C_{dl} *the dlc, and* Z_W *the Warburg impedance* *b)* *Typical response of the Randles circuit in* $(Z', -Z'')$ *plane.*

Another common model (figure 1.14) deals with unsupported binary electrolytes, i.e. solvent and one salt. It takes into account the geometrical capacitance, C_g, the bulk resistance, R_∞, the dlc, C_R, the ctr, R_R, and there is an extra subcircuit of R_A, C_A, and Z_D to describe the adsorption and diffusion process of the reactive species to the electrode. R_A and C_A are the adsorption resistance and capacitance and Z_D is the diffusion impedance. The model assumes only one mobile charge carrier. [113]
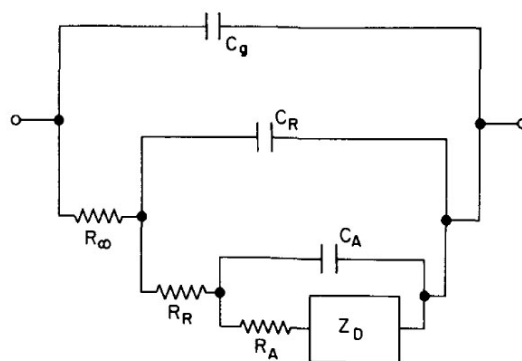
Figure 1.14: *Equivalent model for unsupported binary electrolyte with one mobile charge carrier. C_g is the geometrical capacitance, R_∞ the bulk resistance, C_R the diffuse dlc, R_R the ctr, R_A and C_A the adsorbtion resistance and capacitance, and Z_D the diffusion impedance.*

Additional points

As mentioned earlier, same data can usually be fitted into multiple models. The hierarchial subcircuit models (such as that in figure 1.14) are typically used when one describes intensive behavior, such as processes close to the electrode. On the other hand, series of parallel RC circuits are often used to describe systems with extensive characteristics, e.g. systems with multiple layers or interfaces.

All theory presented in this section applies to half cells. If a non-inert reference electrode or a system of two different types of electrodes (system with only two electrodes) was used, a spectrum that describes both electrodes simultaneosly would be obtained, which is not usually preferred. Those cases are extensive, which means that the series model is used. However, if chemically and geometrically identical electrodes are used, the effects tend to average [92].

Chapter 2

Experimental methods

2.1   Sample preparation

In this thesis gold nanoelectrodes were used to both trap and measure the DNA structures. The used structures had two opposing very narrow fingertip type electrodes with a small gap (as in figure 2.1). The structures were prepared using conventional electron beam lithography, and thus only key steps and factors are presented here. For more details, see appendix A.
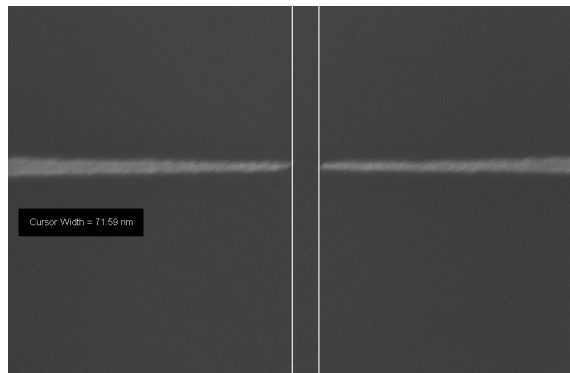
Figure 2.1: *A SEM image taken of a ready finger tip electrode structure. The width of the gap is about 70 nm.*

First, an insulating layer of silicon dioxide was grown thermally on a slightly boron-doped (100)-oriented silicon. The resist used for patterning was a 2% solution (mass percentage) of polymethyl methacrylate (PMMA) in anisole. Spin coating was carried out with a rate of 2000 RPM followed by 5 minutes of baking on a hot plate at 160 ºC. After the exposure, which was done by using an electron beam writer (Raith E-line), the pattern was developed in a solution of methyl isobutyl ketone

(MIBK) and isopropanol (IPA) with 1:3 ratio for 30 seconds at ambient conditions. The development was stopped by rinsing with IPA. After that the exposed area was cleared from left-over undeveloped residues by using reactive ion ecthing (RIE). A short oxygen plasma flash was used to accomplish the goal. This step was crucial to the whole processing because the conductivity of the 20 nm wide gold nanoelectrodes was increased by four orders of magnitude by it, while the patterned lines widened only about 5 nm [115, 116]. The evaporation of titanium and gold films, in respective order, was done in ultra-high vacuum (UHV, pressure of the order of 10^{-8} mbar) chamber equipped with an electron gun. The thickness of the evaporated layer of titanium, to increase the adhesion of the gold, was about 1-2 nm and it was topped with 15-20 nm of gold. After the evaporation the sample was dipped into hot acetone and left there overnight for lift-off. After most of the metal had detached, the sample was shortly sonicated and rinsed using a syringe filled with acetone to remove rest of the residue metal. The samples were then cleaned with IPA and imaged with an optical microscope. An image of a ready structure taken by using a SEM is presented in the figure 2.1. Right before the DEP experiments residues from the lift-off were removed by oxygen flash in RIE. The last RIE flash also makes the originally hydrophobic silicon oxide hydrophilic [7].

2.2 Fabrication of the DNA structures

2.2.1 TX tile B-A-B structures

The majority of the DNA sequences were adopted from previously published structures (see references [58,117]) and modified to our needs. The change of the sequence symmetry and the minimization of undesired complementarity were done by using M-fold web server [118]. The TX tiles used in this work were designed so that only a finite-size complex B-A-B (see figure 2.2 for a schematic presentation and AFM images of the ready structures on mica surface) was able to assemble instead of an infinite array as in the earlier designs. To archieve this only three different kinds of 8-nt-long sticky ends were symmetrically used in the tile A (*a,b,c*) so that it could be rotated 180 degrees still having the sticky ends at the same orientation in the both ends. The tile B had complementary sticky ends (*a',b',c'*) at one end. The sticky ends *d* (12 nt) at the other end of the tile B had identical sequence, and therefore they could all be assembled with complementary strands *d'* containing thiol-groups at the 5' end. The thiol-modifications were added to the tile B for the purpose

of the forthcoming immobilization of the constructs to the gold electrodes via S-Au bonding. The designs of the tiles A and B are presented in the appendix B. The tile A has 16 bp between the crossover points corresponding to 1.5 turns of B-DNA double helices, enabling the same natural orientation for helices when tile B is assembled to either sides of the tile A. [119]
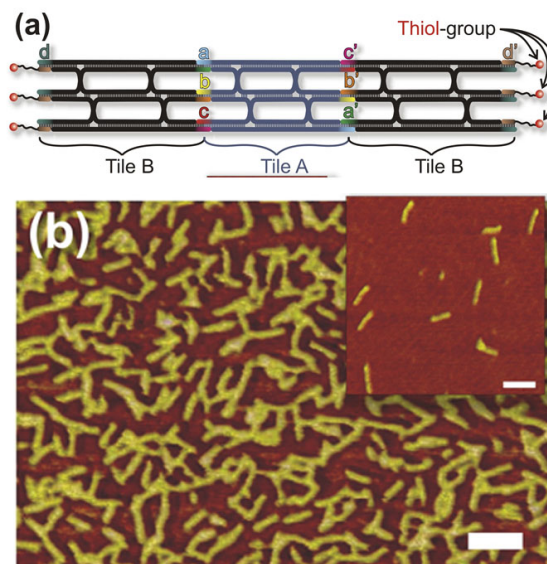

Figure 2.2: *a) A schematic presentation of the B-A-B complex. a,a',b,b',c,c',d,d' are sticky ends so that the ones with the apostrophe are complementary to the ones without (also indicated by the colors). The bridges describe the crossovers. b) An AFM image of the ready complexes on Mica surface in dry conditions. Scale bars are 100 nm. The image is adapted from [119].*

The approximately 10×60 nm^2 complexes were formed in TAE Mg++ buffer [40 mM Tris (pH 7.6), 1 mM EDTA, 19 mM acetic acid (HAc), 12.5 mM magnesium acetate (McAc)] and T4 polynucleotide kinase (New England Biolabs) was used to enable the following ligation procedure, i.e. add phosphates to the 5' end of each DNA strand (PAGE- or HPLC-purified, Biomers GmbH, Ulm, Germany), except the 5'-thiol-modified strand (HPLC-purified, Integrated DNA technologies, Coralville, Iowa, USA). Each strand was modified (see appendix B) separately using T4 polynucleotide kinase with T4 DNA ligase buffer (New England Biolabs) and the strands were incubated for one hour at 37 °C. [119]

To achieve appropriate concentration of each tile, the T4 kinase modified strands were mixed using twofold amount of strands that form tile B compared to strands forming tile A. In addition, threefold amount of 5'-thiol-modified strands were used,

compared to the strands forming tile B in order to hybridize them with each sticky end d of the tile B (in figure 2.2). Complexes were formed by heating the reaction solution (see appendix B) up to 90 °C and cooling it down to 20 °C at a rate of 0.01 °C/s in a PCR-machine (Biometra GmbH, Goettingen, Germany). After the annealing complexes were ligated using T4 DNA ligase (New England Biolabs) to make the complexes more stable for the DEP trapping. The ligation catalyzes formation of phosphodiester bonds between adjacent 5'-phosphates and 3'-hydroxyl terminals of the staple strands in the formed duplex DNA [115]. Mixture was incubated for two hours in dark at room temperature and stored at 4 °C afterwards. The theoretical concentration of obtained complexes was 0.29 μM of A strands (tile A) and 0.58 μM of B strands (tile B). [119]

2.2.2 Rectangular DNA origami structures

The rectangular 71×98 nm^2 origami structures used are made of the genome of M13mp18 virus (New England Biolabs) accompanied with 192 staple strands (unpurified from Integrated DNA Technologies), plus the thiol-modified side strands (Integrated DNA Technologies). The side strands and a schematic picture of the design are presented in Appendix C. Figure 2.3 shows the AFM image of the ready structure on mica surface in liquid conditions (plus a smiley-shaped structure).
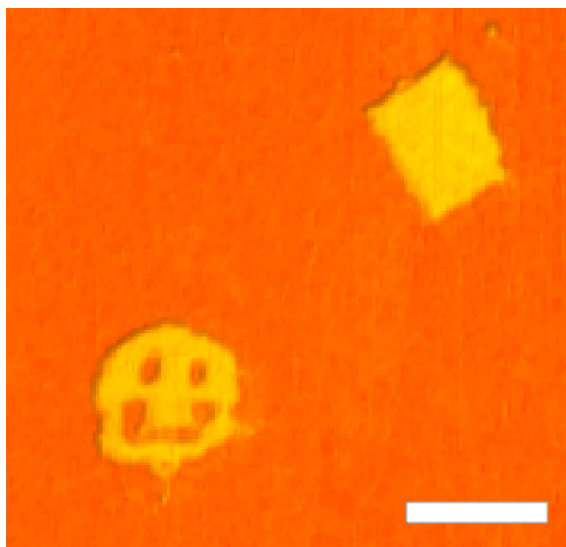

Figure 2.3: *An AFM image with a smiley-shaped and a rectangular origami structure on mica surface in liquid conditions. Scale bar is 100 nm. The image is adapted from* [115, 120].

The structures were formed in a solution of TAE Mg++ buffer [40 mM Tris (pH 7.6), 1 mM EDTA, 19 mM acetic acid, 12.5 mM magnesium acetate], T4 DNA ligase buffer (New England Biolabs), M13 DNA, staple strand mix, thiol-modified side strands, and T4 polynucleotide kinase (New England Biolabs). 10× excess concentration of the staple strand mix (all strands have the same concentration) was used compared to the concentration of the scaffold strand. The solution was first kept for 1 hour at 37 °C (optimal condition of kinase enzyme reaction), then heated up to 90 °C, and finally cooled down to 20 °C at a rate of 1 °C/min in 0.1 °C steps. After the annealing the structures were ligated by adding the T4 DNA ligase (New England Biolabs) and keeping the sample for 8 hours in a dark place at room temperature. The resulting concentration of the origami structures was about 1 nM. [121] See appendix C for the absolute concentrations used in the above procedures.

2.3 Immobilization of the structures

As a final step of the preparation of the structures, the buffers used for annealing and ligation were changed to a Hepes-based buffer (6.5 mM Hepes, 2mM NaOH, 1 mM magnesium acetate, pH∼7) of smaller conductivity (ca. 300 μS/cm) by using spin-filtering. The filtering procedure washes out everything lighter than a certain cutoff weight. The process was crucial to the DEP experiments since the buffer of low conductivity reduces Joule heating (less thermally induced flow) and polarizability of the buffer thus increasing the effective polarizability of the DNA in the buffer [7].

The final theoretical concentration of the B-A-B structures was about 30 nM, but it might be far from reality (diluted to 10% before filtering, all tiles A probably have not formed full B-A-B structures). The structures were stable for only few days when stored in fridge. For origami structures the concentration was 1 nM (not diluted before filtering, almost all structures recovered from the filter) and they were stable at least for a week when stored at room temperature. For more information about the filtering process, see appendix D.

The DEP was done inside a metallic box equipped with feed-throughs connected to a signal generator. The sample chip was put on a nylon (covered with epoxy) support, after which small sharp metallic probes were connected to the pads of the sample. A 10 μl drop of the DEP buffer containing the DNA structures was dropped on the sample, more precisely on the fingertip electrodes. The drop spread evenly on the chip because the surface was made hydrophilic. Water was added
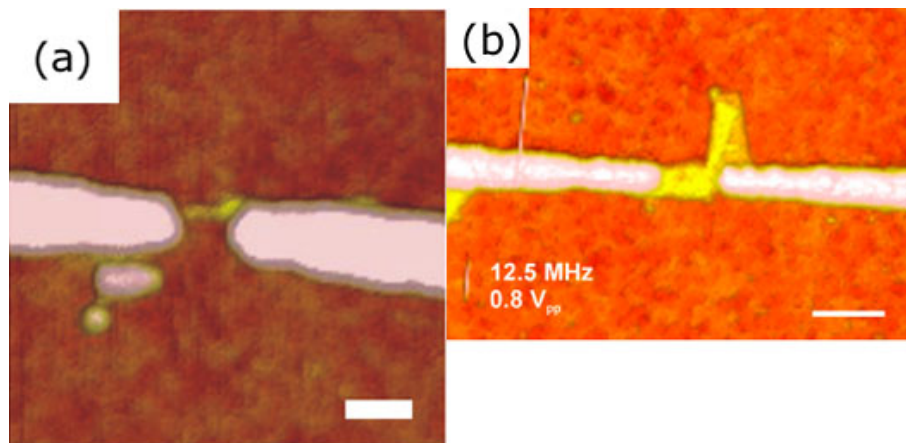
Figure 2.4: *a) A single TX tile structure trapped in the gap. The scale bar is 50 nm. **b)** A single origami structure trapped in the gap and another next to the gap. The scale bar is 100 nm. The images are adapted from [119] and [115, 120], respectively.*

to the box to increase humidity, i.e. to prevent the DNA drop from drying during the DEP. Time required to succesfully trap one or more structure(s) was about 5 minutes. After the DEP the samples were first rinsed gently with Hepes-NaOH (3 mM Hepes, 2 mM NaOH) to remove excess magnesium, then with distilled water, and finally gently dried by using nitrogen flow. Samples were imaged using AFM (Veeco Dimension 3100) to see if any structures had found their way into the gap and attached to the electrodes. Figure 2.4 shows successful immobilizations.

An important observation is that the height of the origami structures in dry conditions on silicon oxide is about 2 nm [115], whereas the height of the B-A-B complexes varied. The maximum height was about 1.5 nm and the minimum about 0.6-0.7 nm (see figure 2.5). The typical height of dsDNA molecules on the substrate is 0.5 nm-1.5 nm [53].

Hundreds of samples with gaps of 70-90 nm were used to optimize the trapping parameters for the origami structures. After that about 30 samples with gaps of 45-65 nm were used to get enough information to trap the TX tile structures. The optimal parameters, i.e. frequency and peak-to-peak voltage, for the former were 12.5 MHz and 0.8 V, and for the latter about 11 MHz and 1.5 V.
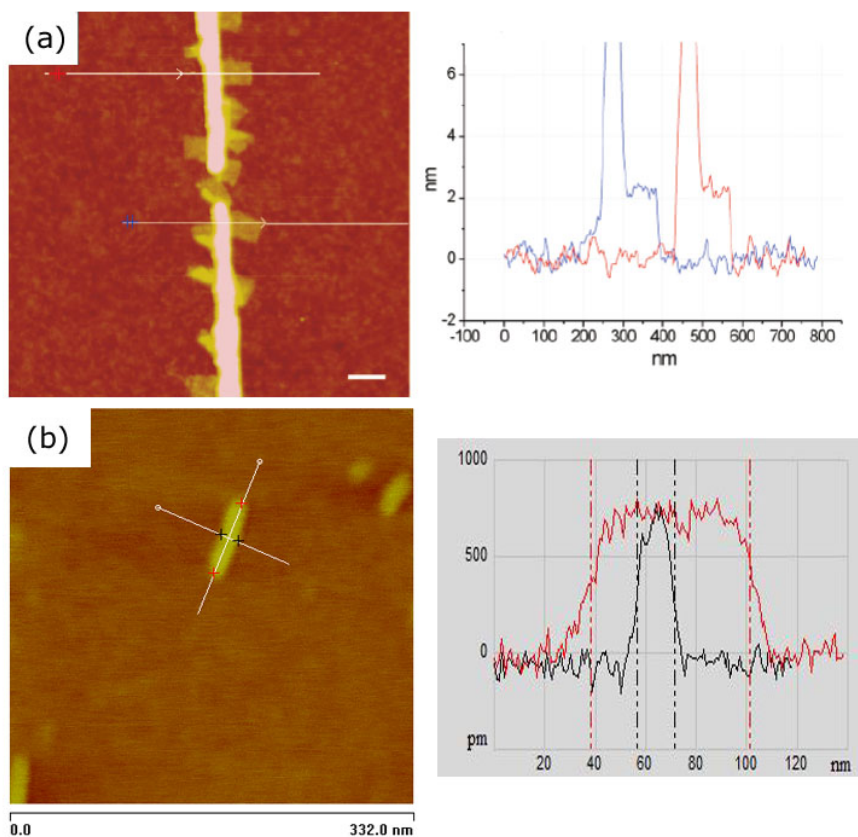
Figure 2.5: *a) Dimensions of origami structures measured near the electrodes. The height of the origami structures is about 2 nm. The scale bar is 100 nm. The image is adapted from [115, 120]). b) Dimensions of a TX tile structure measured on silicon dioxide. The length is about 63 nm, width 15 nm, and height 6-7 Å.*

2.4 Measurements

2.4.1 DC measurements

Successful immobilization of a single DNA structure made it possible to measure its conductivity. The measurements were carried out inside an electromagnetically shielded (EMS) room equipped with highly-filtered and optically isolated feedthroughs. Furthermore, the samples were put on the nylon stage into a metallic casing with feed-throughs for signal cables, pumping, and humidity and nitrogen supply. Humidity was obtained by slowly boiling distilled water in an oil bath and using plastic hose to cool down the vapor and lead it to the casing. All the measurements were done in room temperature and the temperature varied only few degrees during the measurements (cooled in all the cases).

Current-voltage (I-V) characteristics were obtained by sweeping a DC bias voltage, produced by a battery-powered DAC circuit controlled via optical lines, in finite steps from -0.3 V to 0.3 V. The low voltages were used to prevent unwanted effects, e.g. breakdown of the sample due to excess heating, electrolysis, and gathering of contaminating particles from the air. A low-pass RC filter (resistance 100 Ω, capacitance 47 μF) was used to protect the sample from high frequency transients of the bias voltage. The current and voltage were measured using battery-powered preamplifiers (DL-Instruments Model 1211 and DL-Instruments Model 1201, respectively). Relative humidity (RH) and temperature were measured using Honeywell Humidity sensor (HIH-3602-A). The signals from the preamplifiers were fed to a computer through a data aquisition card (DAQ, National Instruments PXI-1031). See figure 2.6 for a schematic presentation of the measurement setup controlled by a homemade Labview program that was also used to record and visualize the data. The system had 500 ms to settle after each voltage step. The DAQ rate used was 10.000 scans/s and 1000 points were averaged per each recorded value.

All the samples were measured in both dry (RH less than 5%) and humid (RH 80-90 %) conditions since DNA should be in its natural B-form (13 water molecules per nt required) when the RH is close to 90 % [121, 122]. Yet, the humidity is not too high to allow significant condensation of water on top of the sample.

In the case of the origami samples current-RH (I-RH) characteristics were measured using a bias voltage of 0.3 V, whereas conductance-RH (σ-RH) characteristics were measured for the TX tiles by slowly increasing the humidity while sweeping the DC voltage.

2.4.2 AC measurements

The AC measurement setup was otherwise the same as in the case of the DC measurements (see 2.4.1 and figure 2.6), but the measuring and feeding devices were completely different. Two lock-in amplifiers (Stanford Research 830), equipped with GPIB, were used to measure the voltage and the current signals. The one measuring the voltage also fed the system with a small sine signal (50 mV RMS amplitude, with a maximum deviation of 10% and constant phase) from its signal generator. Both amplifiers locked into the frequency of that signal. Two battery powered preamplifiers (HMS Electronics, Model 568) were used to give the voltage signal the 10$\times$ gain and to increase the input impedance to avoid extra voltage division. The DAC circuit with the low-pass filter was added to the setup when also a DC bias voltage
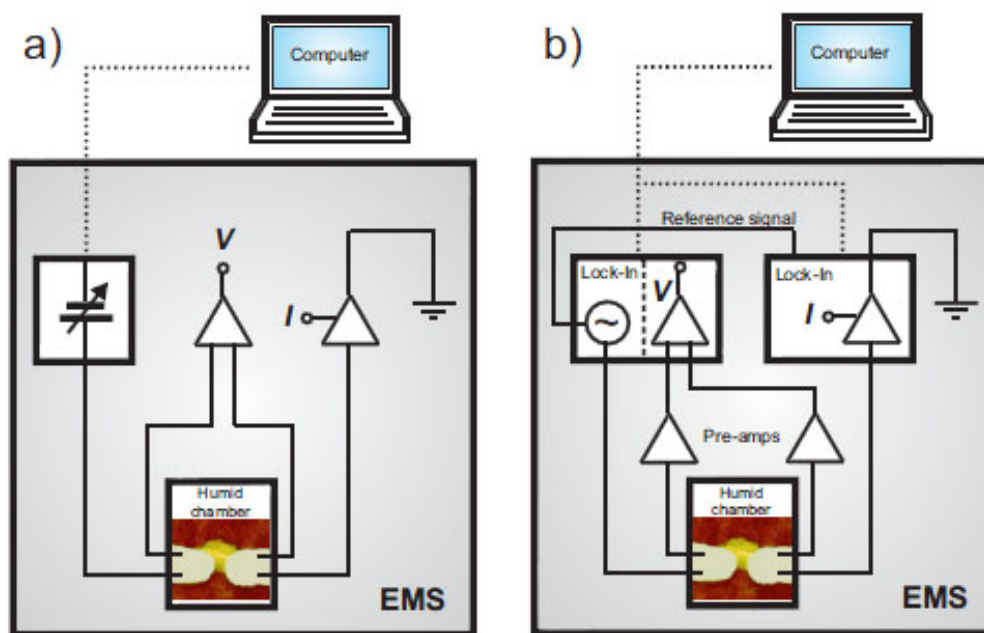
Figure 2.6: *A schematic presentation of the measurement setups used in **a)** DC measurements and **b)** AC measurements.*

was needed.

Higher frequencies, about 1 Hz-100 kHz, were always measured first. At the higher frequencies the lock-in amplifiers were able to automatically adjust their ranges, whereas below 1 Hz those had to be manually set. Thus the measurements were always done in two or three parts (e.g. 0.01-1 Hz, 0.5-5 Hz, 1 Hz-100 kHz) so that the frequency ranges overlap. Required adjustments to measuring parameters were done between the parts (see appendix E for an example).

Before measuring the immobilized DNA structures, measurements were performed in dry conditions for dry clean electrodes to determine the stray capacitance and the small leakage current (of the system) parallel to it. Rest of the measurements were performed in humid conditions (RH≈ 90%). The obtained data was fitted using CNLS-method by exploiting LEVMW 8.08 (freeware) software [123].

Chapter 3

Analysis and results

Most of the data, results, and figures in this chapter have been adapted from references [119, 121] with permission. Samples measured are divided into three categories: empty, control, and DNA samples. The empty samples contain no DNA and have not undergone any chemical treatment assosiated with the DEP trapping. The control samples underwent the same DEP trapping and the following washing procedures as the DNA samples but without any DNA in the trapping buffer.

3.1   DC conductivities

Empty dry samples showed a resistance of the order of $\sim$100 TΩ, which means that the oxide layer is insulating as it should.

Both the TX tile and origami structures showed a resistance of the order of $\sim$TΩ when dry, which confirms that the intrinsic electronic conductivity is negligible.

I-RH and σ-RH characteristics were measured for origami and TX tile structures, respectively (figure 3.1). The control samples show exponential behavior in both cases, which can be adressed to water being the main charge carrier [124] via adsorption of water molecules and Grotthuss mechanism. In the case of the TX tile structures it was noticed that the conductance did not increase significantly although RH increased from $\sim$5 % to $\sim$60 %, but after 60 % the behavior is almost exponential. The case of origami structure, on the other hand, shows increased conductivity even at lower RH levels. The difference between origami and TX tile samples could be due to the ability of the origami structure to hold its level of hydration (and thus its conformation) even at dry conditions, as confirmed by the heights measured by AFM imaging (see 2.3).

The DC sweeps of the control samples at humid conditions (RH=90%) show
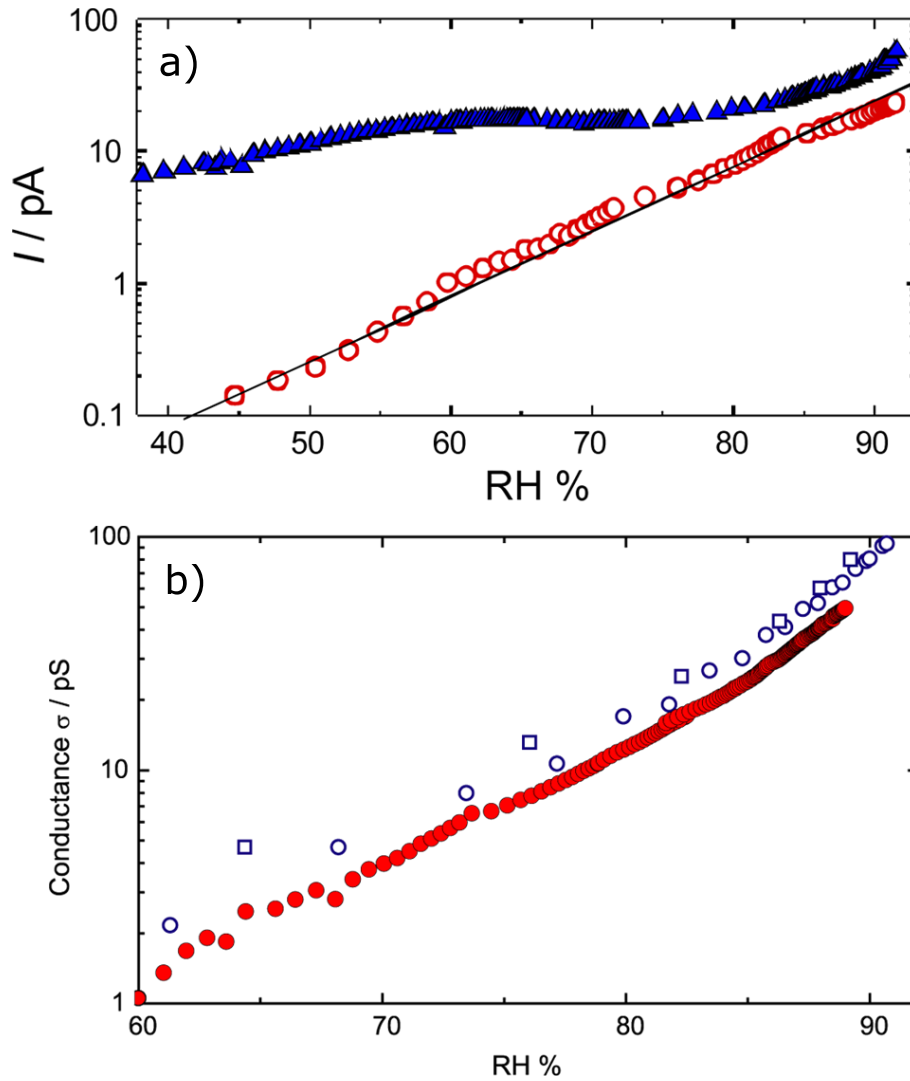
Figure 3.1: *a)* *The I-RH (with 0.3 V bias) characteristics for an origami sample (blue triangles) and a control sample (red circles).* *b)* *The conductance characteristics of TX tile samples (open blue circles and squares) and a control sample (red cirles). The images are adapted from [121] and [119], respectively.*

almost ohmic behavior with a resistance of about 30 GΩ or more (figure 3.2). The origami samples show S-shaped, non-linear behavior with a resistance of about 10 GΩ between -0.2 V and 0.2 V and about 2 GΩ outside this region. The TX tile sample, on the other hand, shows a bit higher resistance of about 20 GΩ between -0.2 V and 0.2 V and about 15 GΩ outside.

Both samples exhibit hysteresis (figure 3.2), which in the case of the TX tile sample is due to the step-like charging of the total capacitance of the system [53,119].
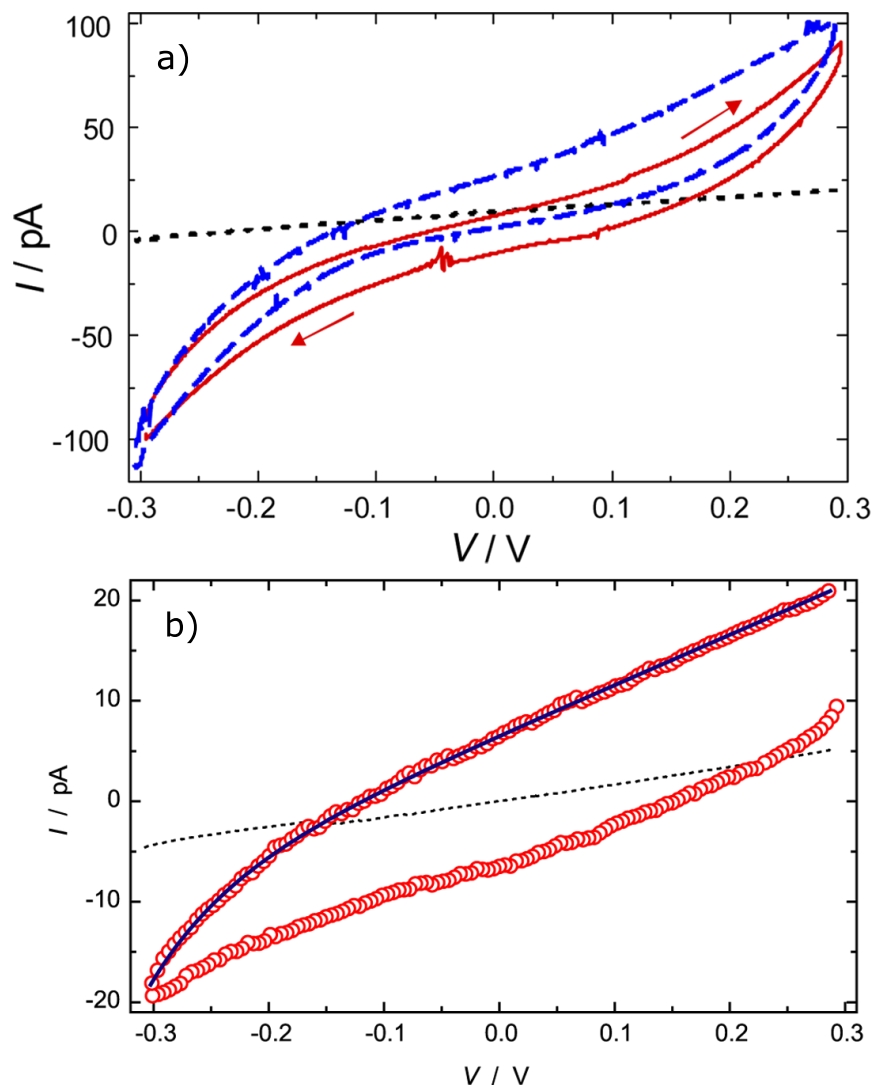
Figure 3.2: *a) The I-V characteristics for two origami samples (blue dashed and red solid line) and a control sample (black dashed line). The arrow indicates the direction of the voltage sweep. b) The I-V characteristics of a TX tile sample (red solid line) and a control sample (black dashed line). The hysteretic behavior is due to enhanced charging at the high humidity as shown by fitting a linear IV dependency with charging effects included to the data (solid blue line). Both have been measured at RH=90 %. The images are adapted from [121] and [119], respectively.*

The data can be fitted to an equation of the form

$$I = \frac{V_{\mathrm{n}}}{R} + I_0 \alpha \frac{1 - \alpha^n}{1 - \alpha}, \tag{3.1}$$

where I is the current, n the nth point measured, V_{n} the corresponding bias voltage, R the resistance of the sample, I_0 the maximum charging current at bias voltage transients (depends on the resistances of the measurement instruments), and $\alpha = \exp(\tau_{\mathrm{m}}/\tau)$ the exponential of the ratio between the stabilization time (500 ms in our measurements), τ_{m}, and the time constant of charging, τ. The fitting [figure 3.2(b)] gave out a resistance of 20 GΩ and a time constant of 70 s.

The case of the origami samples (figure 3.2b) is a bit different because of the S-shaped I-V curves. It appears that the bias voltage of 200 mV is enough to enable some nanoscale electrochemical effect, e.g. oxidation of gold, or increased electronic conductivity [42] via thermal hopping through random barriers. Gold is the noblest of metals, but it should oxidize to trivalent state with a standard potential of about 1.5 V. Nevertheless, it has been observed and theorized that gold, especially nanoscale gold aggregates or surface defects, can be much more reactive than their bulk lattice equivalents and thus oxidize at very low potentials [125–127]. It is to be noticed that the exponential dependence of conductivity as a function of RH (figure 3.1) was also reported for porous oxide materials and attributed to the adsorption of water molecules on the film surfaces [124, 128].

The low DC-conductivity of the origami samples could be explained by the high resistance of the linker groups consisting of thiol-modified $(CT)_{16}$ single strand sequence. The resistance of the hexanethiol has been reported to be about 10 MΩ near zero bias [129], and moreover it has been observed (due to the fact that there is no possible conduction channel via base stack) that ssDNA molecules are poor conductors [124]. On the other hand, the TX tile structures have no ssDNA spacer, and yet the result is almost the same, which suggests that charges cannot use the Au-thiol-DNA bridge to enter the base stack or the intrinsic conductivity is negligible. It is not even clear how the work function of Au (~ 5 eV) relates to the LUMO of random DNA, but it is believed that it is below, i.e. DNA might act as an energy barrier for electrons between gold electrodes [51]. Nevertheless, a known fact is that the work function of Au is decreased significantly in aqueous solution [130, 131].

3.2   AC-IS measurements

Since the DC measurements do not give any reliable information about the possible electronic conductivity or conduction mechanisms of the DNA structures, AC-IS was utilized.

3.2.1   The stray capacitance

Before measuring the impedance spectrum of the control and DNA samples the stray capacitances and the leakage currents of the measurement setup were determined by measuring a dry empty sample followed by fitting the data with an equivalent circuit comprised of a resistor and a CPE in parallel. The fitting yielded a leakage resistance of about 0.1-0.3 TΩ and proved the CPE to be almost an ideal capacitor [i.e. $\gamma \approx 1$, see equation (1.20)] with a capacitance of about 6.8-9 pF (fitting results shown in the table 3.1).

3.2.2   The control samples

Before measuring the DNA samples, it was necessary to find an equivalent model describing the control samples at RH=90 %. Tens of models were tested by fitting the data and comparing the goodnesses of the fits. The circuit that gave the best fit is shown in the figure 3.4a. The model contains two serial impedances, Z_s (green) and Z_dl (blue), in parallel with the stray capacitance C_e. The leakage current is omitted from the model because of its high resistance value. The two impedances had to be in series since the parallel versions of the models were less physical.

Typical $(Z', -Z'')$ plots obtained for the control samples used in the origami (OC1) and TX tile measurements (TXC1) are shown in figures 3.3a&c, respectively. The circuit (figure 3.4a) produces essentially two, or two almost convoluted, depressed semicircles.

Both impedances are comprised of a CPE and a resistor in parallel during the fitting. One CPE turns out to be like an ideal capacitor (called C_dl) while the other CPE has $\gamma \approx 0.5$ [see equation (1.20)] and is called W_diff. The CPEs are accompanied by resistances called R_ct and R_s, respectively.

The component C_dl is thought to describe the vicinity of one electrode, i.e. the dlc formed by water molecules first covering the gold electrode (via van der Waals forces) and then small ions (e.g. protons, hydroxide ions, or ionized salts from the left-over DEP buffer) screening the surface charge (see section 1.5.3 for discussion about
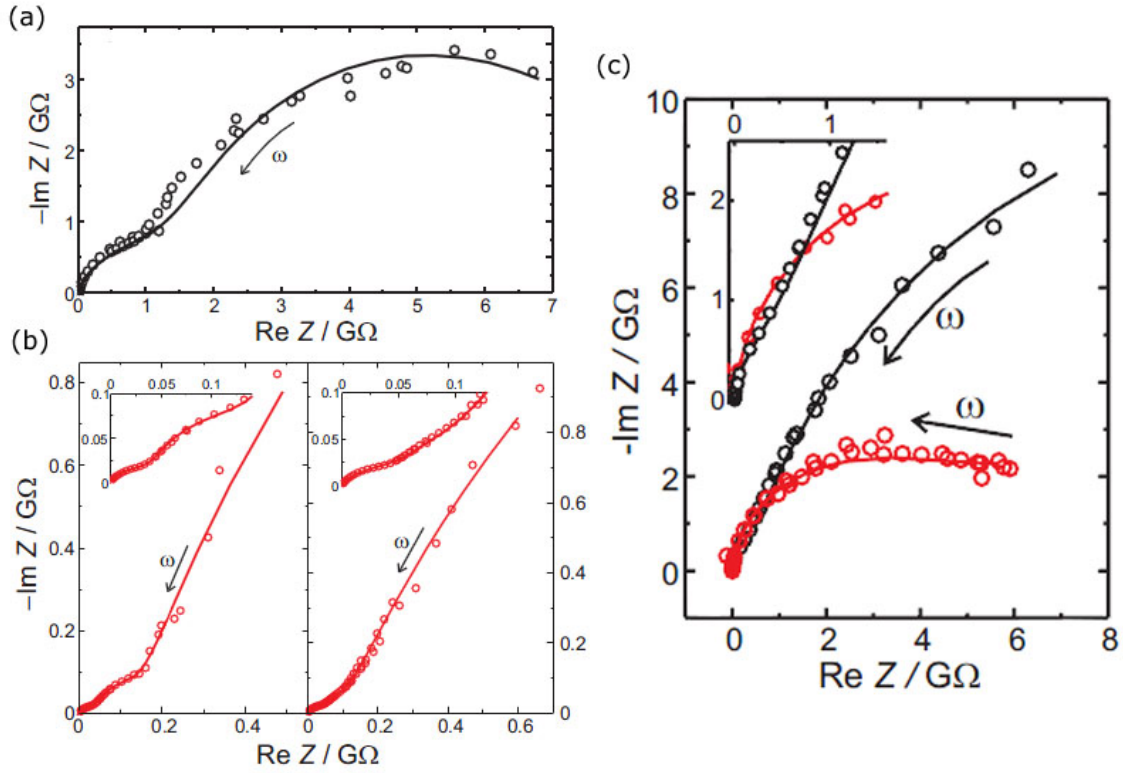
Figure 3.3: *a) (Z′,−Z″) plots and data fittings for a typical control sample (OC1, black circles and black curve) used in the origami measurements, b) (Z′,−Z″) plots and data fittings for two different samples (O1-O2) containing a single rectangular DNA origami (red circles and red curves), c) Plots and data fittings of a control sample (TXC1, black circles and black solid curve, respectively) used in the TX tile measurements and a sample (TX1) containing a single TX tile construct in the gap (red circles and red solid curve). The images a) and b) are adapted from [121] and b) from [119].*

double layers).

The resistance R_{ct} describes the total electronic charge moving through the DL. No typical electrochemical reactions should occur between the gold and the water or ions with the zero bias and the small excitation signal used. Thus the electronic transport must be mostly due to thermal tunneling through the SL.

At this point, it should be noted that the Debye length [see equation (1.15)] (aqueous solutions) for our system can easily be of the order of ∼100 nm (approximated by using the relative permittivity of water and ionic strength of the order of 10 mM) or even more, which means that the diffuse layers of the two DLs of the electrodes overlap. Therefore, it should be clarified that the electron tunneling takes place in the SL.
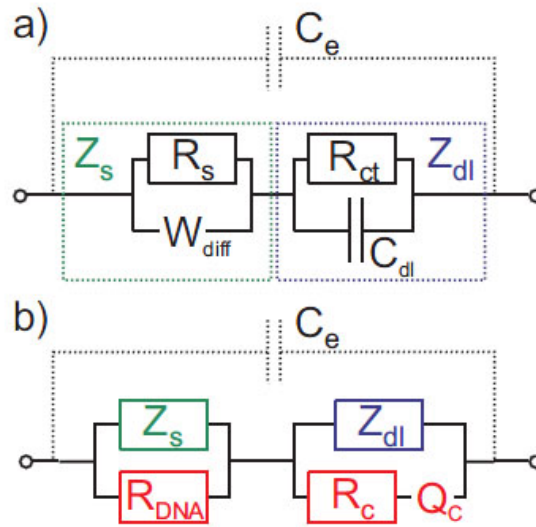
Figure 3.4: *The equivalent circuit for **a)** control samples and **b)** DNA samples. C_e=the stray capacitance, Z_{dl}=the impedance of the SL (blue), Z_s=the impedance of the diffuse layer (green), C_{dl}=the dlc of the SL, W_{diff}=the unideal capacitance of the diffuse layer described by a CPE, R_{ct}=the ctr of the SL, R_s=the resistance of the diffuse layer, and R_c together with Q_c=the contact impedance between the construct, linker, and electrodes or the changes in the SL. The image is adapted from [121].*

R_s is attributed to the losses (solution resistance) in the electrolyte solution, i.e. the migration and diffusion of charged species in the diffuse layer under the applied potential difference, whereas W_{diff} describes the capacitive properties of that region. The component is, in my interpretation (see [119, 121] for a different point of view), misleadingly named after the Warburg diffusion impedance [see equation (1.21)] because of the exponent of the CPE. A CPE rather describes a very distributed capacitive behavior than losses due to linear diffusion when connected in parallel with a resistor [92].

All the above components and the corresponding values obtained from the fittings are shown in the table 3.1.

3.2.3 Full model

The model used to fit the data of the DNA samples is shown in figure 3.4b. The model is a modified version of the model for the control samples (figure 3.4a). Data from three separate origami samples (O1-O3) and one TX tile (TX1) is fitted and compared to the control samples (see table 3.1).

The plots obtained from samples O1-O2 and TX1 and the data fittings based on the used model are presented in figures 3.3b&c. Similarly to the control samples the semicircles are again visible, but now there exists an additional low frequency tail.

The impedance describing the processes (assumed to be mostly tunneling) in the SL of the control samples, Z_{dl}, is modified by adding a serial combination of a resistor (R_c) and a CPE (Q_c) with varying exponents (n_Q from 0.3 to 0.8) in parallel. It is obvious that the charge transfer through the SL gets altered when a DNA molecule is attached electrically, chemically (covalently via linkers), and mechanically (brought to physical contact) to the gold, but the mechanism of the CT is not completely clear. It appears that the tunneling process through the SL (described by R_c) is significantly eased at the high frequency limit but is limited by the impedance of the CPE, Q_c, at low frequencies. Since the Q_c does not formally have a DC limit, the R_{ct} included in the Z_{dl} will take care of that.

A resistance, R_{DNA}, is added in parallel with the impedance Z_s describing the diffusive layer that is now filled with DNA.

3.2.4 Observations and discussion

Common differences between the control and DNA samples

In the DNA equivalent circuit the large resistance R_{ct} is still present in the circuit but has a negligible contribution to the AC conductivity since it is large compared to other impedances parallel to it. However, at low frequencies, i.e. close to the DC limit, it plays a significant role. Formally, the impedances of Q_c and C_{dl} are infinite at the DC limit, and thus they can not describe a possible small electronic DC current flowing directly from the DNA, or via the linker, to the electrode. The resistance describing such a small current would be parallel to R_{ct} and can be understood to be included therein. During the fittings it was noticed that the value of R_{ct} was similar to the control sample, which implies that the resistance related to the direct electronic DC current from the DNA to the electrode is larger than the value of R_{ct} determined for the control sample. By adding R_s and R_{ct} from table 3.1 together, one can estimate the DC resistance of the equivalent circuit to be roughly 10 GΩ, in case of the origami samples, or 25 GΩ, in case of the TX tile sample, which agrees with the measured DC resistances near zero bias. A simple DC measurement is not enough to characterize the conductivity since the large resistances hide crucial information about other possible conductivity mechanisms.

Table 3.1: *The fitting parameters obtained for the equivalent circuits for the control samples (OC1 and TXC1) and the DNA origami (O1-O3) and TX tile (TX1) samples. The values in the parentheses are not fitted but fixed, based on the fitting of the dry or control samples, or for other reasons (described in the text). The data is adapted from [119, 121].*

Sample (V_{bias}, RH)	$R_{\mathrm{s}(\|\mathrm{DNA})}$ [MΩ]	W_{diff} [ps$^{\frac{1}{2}}\Omega^{-1}$]	C_{dl} [pF]	R_{ct} [GΩ]	R_{c} [MΩ]	Q_{c} [ps$^{n_Q}\Omega^{-1}$]	n_{Q}	C_{e} [pF]
OC1 (0.0 V, 90 %)	2200	110	290	7.4	-	-	-	(9.0)
TXC1 (0.0 V, 90 %)	1300	13	26	26	-	-	-	(6.8)
O1 (0.0 V, 90 %)	60	1100	1100	(7.4)	120	5.3	0.79	(9.0)
O2 (0.0 V, 90 %)	83	1200	1800	(7.4)	73	4.6	0.71	(9.0)
O2 (0.3 V, 90 %)	69	1000	1500	2.8	66	3.7	0.77	(9.0)
O3 (0.0 V, 95 %)	67	2700	20	(∞)	41	7.4	0.50	(9.0)
TX1 (0.0 V, 90 %)	900	29	1.8	(26)	1500	0.13	0.3	(6.8)

However, the resistance describing the parallel combination of R_{s} and R_{DNA} is significantly smaller than R_{s} of the control sample (OC1) in the case of the origami samples (O1-O3), whereas the TX tile sample (TX1) shows pretty similar (a bit lower) resistance to the control sample (TXC1). If it is assumed that the thermal hopping is negligible, the lowered resistance could be due to intrinsic conductivity or increased ionic conductivity.

The constant W_{diff} of samples O1-O2 is about tenfold increased compared to the control sample (OC1). The case of the TX tile sample (TX1 compared to TXC1) also shows slight increase.

The simultaneous increase of W_{diff} and R_{s} can be explained by simultaneous increase of permittivity and ionic conduction along the DNA via H^+ and OH^- ions produced by the water adsorption of the DNA. The charges separate and recombine according to Grotthuss mechanism. The ionic conductivity via this mechanism is dependent on both the RH and the permittivity [124]:

$$\sigma \propto \sqrt{N_{\mathrm{w}}} \exp\left(\frac{-q^2}{2\epsilon_{\mathrm{r}}\epsilon_0 dRT}\right), \tag{3.2}$$

where N_{w} is the amount of water molecules adsorbed per nucleotide, and the exponential function describes the amount of energy required to separate the charge species (q is the charge, d the equilibrium distance of the charge species).

The roles of R_{c} and Q_{c} remain a bit unclear. The R_{c} is probably due to enhanced electronic transfer because of e.g. increased amount of protons and hydroxyl ions

near the electrode, lowering of the energy barrier related to the SL, or the linkers. In that case it is only natural that Q_c would describe the processes involved in the polarization of the DNA (and the counterion cloud) surrounding it, which would hinder the combining of charge species, adsorbtion of water by the DNA, and/or the Grotthus mechanism after the tunneling. It can be speculated that the polarization of the medium could have a similar effect also in the case of the control samples (although it takes longer due to lower motility of the charge species), which accually might be the case, but because of the frequency range used (due to the limitations of our measurement setup) it is not observed. The DC limit is governed by fully polarized situation described best by the model of the control samples, i.e. it behaves as if there was no DNA in the gap.

Differences between the DNA samples

On the other hand, C_{dl} of the samples O1-O2 is slightly increased, whereas for TX1 it is tenfold decreased. The difference in the way that the structures influence the SL is probably due to the very different sizes of the constructs and the chemical compositions of the structures.

It has been theorized that the bound water layer around DNA (about 3 Å thick) has lower permittivity than the bulk water due to reduced motility of water molecules [124], which means that the possible conduction channels have to be larger than 3 Å, which in turn implies that the construct with less pores and seams could be less conducting, which is in agreement with the fact that the TX tile structure is seamless. Furthermore, a stretch of DNA nucleotides can adsorb only a certain number of water molecules at a given RH level, and the origami and TX tile structures indeed have very different amount of nucleotides: 14,000 and 1,000 nucleotides, respectively.

By using the relation of linear ohmic resistance, i.e.

$$R = \rho \frac{l}{A}, \tag{3.3}$$

where R is the resistance, ρ the resistivity, l the length, and A and the cross-sectional area of the conductor, a 1:10 ratio of resistances is found between the origami and the TX samples, which roughly agrees with our DC measurements and the discussion in the previous paragraph.

The effect of the bias voltage on sample O2

Furthermore, it was shown (sample O2) that the bias voltage of 0.3 V which is in the high-conductance region of the DC measurement (figure 3.2) reduced essentially only the value of R_{ct}, which implies that the bias voltage does not affect the conduction (ionic or electronic) along the DNA, but instead increases the rate of electrons entering the medium, which in turn eliminates the possibility of enabled thermal hopping along the DNA (at least at this low voltages). Thus the origin of the increase of conductivity is attributed to electrochemical effects at the electrode surface or just eased electron/hole tunneling.

The effect of further increasing humidity on sample O3

The influence of further increasing RH to 95 % was also investigated (sample O3). It is clear that the water is remarkably affecting the conductivity since the value of W_{diff} is about doubled, whereas C_{dl} is almost hundredfold decreased, which means that the composition of the SL must get drastically altered. In addition, the exponent of the Q_{c} changed from ~0.8 to 0.5, which could be attributed to more idealized diffusion, possibly along DNA. The resistance R_{s} remained almost the same.

Differences between the control samples

By comparing the two control samples TXC1 and OC1 it can be seen that even though the values of R_{s} imply that the ionic strengths of the control samples are about the same, the values of R_{ct} differ tenfold. This could be due to slight differences in pH, which in turn could be attributed to combination of the tunneled electrons with the protons in the vicinity of the electrode. The other possibility is hole tunneling and combination with hydroxyl ions. Furthermore, the gap sizes of two control samples are different, and the dimensions of the gold electrodes might also differ.

Additional points

The solution resistance of strong electrolyte solution (full dissociation) with no ions with higher valence numbers is given the Kohlrausch's law for molar conductivity [132]:

$$\lambda_{\text{m}} = \lambda_{\text{m}}^0 + K\sqrt{c}, \tag{3.4}$$

where λ_{m}^0 is the limiting molar conductivity, K an empirical constant, and c concentration (generalizes to ionic strength via activities of different species). Thus the solution resistance is roughly inversely proportional to the ionic strength of the electrolyte solution, which can be assumed to be roughly the same between the control and DNA samples (depends on the washing procedure, which was kept the same all the time). Therefore, the large variations in the conductivity between the DNA samples and the control sample cannot be only due to changes in the ionic strength.

When interpreting the results a few things should be taken into account:

- The data available is very limited because of the limited time, resources, and rather low yield of trapping (only ∼10 % yield with origami and ∼1-5 % with TX tile structures). Hundreds of samples were fabricated because the samples could not be reused due to left-over impurities from the DEP trapping process.

- There is no simple theory for our highly complicated system, i.e. solvent could be gaseous (although the water vapor probably forms a liquid continuum between the electrodes at high RH, see reference [133]), electrode reactions are very slow, bias voltages used are low, electrode separation is much smaller or comparable to the Debye length, solvent is the main charge carrier, and there is a presence of ions with multiple valence numbers.

- All the effects happen in nanoscale, which means that there can be many effects that have not been taken into account, i.e. AC electro-osmosis and the effect of the DL overlapping with it [134], Joule heating, and the very nonuniform electric field.

Chapter 4

Conclusions and discussion

DEP trapping technique can be used as a tool to immobilize single DNA constructs, which enables electrical measurements. The electrical properties of DNA constructs were characterized by means of AC-IS and DC measurements. The developed equivalent circuit model together with the DC measurements describes the processes contributing to the overall conductivity.

The results indicate that the intrinsic electronic conductivity, as well as ionic conductivity, are very low in both dry (electronic conductivity $\sim$ TΩ from DC measurements) and humid conditions (ionic conductivity $\sim$ 100 MΩ from AC measurements), and the main charge carriers in humid conditions are the adsorbed and ionized water molecules, which leads to size dependency and is in agreement with the findings of few other groups [15, 124, 135]. Furthermore, the effect of DL noise due to charging and slow electron transport between gold and water (with or without DNA), was found to hide crucial information about the conductivity in DC measurements, which is not surprising considering that pure water is poorly conducting and the main mechanism turns out to be water-mediated.

The tunneling through water has been studied both theoretically and experimentally [136–139]. Orientation of the water dipoles seems to greatly affect the tunneling rate, and the process can be described as tunneling through a rectangular barrier when the energies are below the energy of the barrier. The effects of water on molecular junctions have been only recently investigated in more detail [122, 140], and it seems that the water produces gating effects on polar molecules due to time-averaged net dipole fields. In this thesis the effects due to dipole relaxation of water were considered negligible since the timescale of such effects (for pure water) is less than one microsecond [141] (largest frequencies measured 100 kHz corresponding to 0.1 μs).

The rate of electron transfer between gold and water is probably very sensitive to changes in pH. In addition, the amount of left-over ions can drastically change the electrochemical kinetics, or even induce ion-gated transport properties in smaller DNA molecules [142]. Therefore, more sophisticated methods to better control the concentrations and pH in nanoscale are required if such effects were to be investigated in more detail.

The DC measurements performed by Tuukkanen *et al.* for 140-nm-long dsDNA molecules using the exactly same methods agree with our (and many other groups) DC measurements in dry [85] on SiO_2 surface. In humid conditions they measured resistances of the order of 100 MΩ-1 GΩ, which does not agree with our result about the size dependency, i.e. larger structures should be more conducting due to increased adsorbtion of water. This could be due to the issues discussed in the previous paragraph, or there was intrinsic conductivity present. The hysteresis is similar to that observed in the case of TX tiles and the time constants of charging ($\sim$ 5-30 s [7,85]) roughly agree with our result 70 s for the TX tile sample, which implies that the former is the better explanation.

Conductance measurements of short DNA strands have taken huge steps forward towards more reliable reproducible measurements and relatively high currents have been obtained [25, 43, 130]. In the first reference cited controllable break junctions were used [143] with a novel thiol modification [144]: the terminal T bases were modified to contain protected thiol groups instead of the backbone. Resistance of about 70 kΩ was measured for 21-bp-long poly(GC) strands in vacuum. In the second reference exponential dependence of the conductivity on the length of the sample containing AT sites was demonstrated. In addition, inverse dependence was found on the length of strands containing only GC sites. 14-bp-long poly(GC) strands had a resistance of about 32 MΩ, whereas the 12-bp-long strands containing GC sites with eight AT bp in the middle showed a resistance of about 2.7 GΩ. The measurements were performed in aqueous solution. The cases containing the AT bp in the middle had a decay constant of $\beta \approx 0.45$ Å^{-1}, which means that the strands are something between an insulator and a wire. The third reference shows large currents through bundles of 26-bp-long dsDNA strands washed with water right before the measurements with bias voltages over 1 V. The last reference is the least reliable since it involves huge voltages that very likely induce electrolysis and tunneling effects.

In conclusion, our measurements indicate that larger DNA structures are dielectrics. Nevertheless, knowing the conductivity mechanism of larger DNA tem-

plates is crucial e.g. from the viewpoints of nanomanipulation, fabricating locally conducting parts by doping, and using the DNA template as a dielectric as such.

Bibliography

[1] J. Watson and F. Crick, "Molecular structure of nucleic acids," *Resonance*, vol. 9, pp. 96–98, 2004. 10.1007/BF02834980.

[2] T. de Bizemont, J.-S. Sun, T. Garestier, and C. Helene, "New junction models for alternate-strand triple-helix formation," *Chemistry & Biology*, vol. 5, no. 12, pp. 755 – 762, 1998.

[3] M. Lu, Q. Guo, and N. R. Kallenbach, "Thermodynamics of g-tetraplex formation by telomeric dnas," *Biochemistry*, vol. 32, no. 2, pp. 598–601, 1993. PMID: 8422371.

[4] C. R. Calladine, *Understanding DNA: The Molecule & How It Works*. Academic Press, 3rd ed., 2004.

[5] X. Hou, W. Guo, F. Xia, F.-Q. Nie, H. Dong, Y. Tian, L. Wen, L. Wang, L. Cao, Y. Yang, J. Xue, Y. Song, Y. Wang, D. Liu, and L. Jiang, "A biomimetic potassium responsive nanochannel: G-quadruplex dna conformational switching in a synthetic nanopore," *Journal of the American Chemical Society*, vol. 131, no. 22, pp. 7800–7805, 2009.

[6] S. Colowick, J. Abelson, N. Kaplan, M. Simon, L. Kuo, D. Olsen, and S. Carroll, *Methods in Enzymology: Viral Polymerases and Related Proteins*. Academic Press, 1996.

[7] S. Tuukkanen, *Dielectrophoresis as a tool for on-chip Positioning of DNA and electrical characterization of nanoscale DNA*. PhD thesis, University of Jyväskylä, 2006.

[8] J. Walker and R. Rapley, *Molecular biomethods handbook*. Humana Press, 2nd ed., 2008.

[9] W. Coleman and G. Tsongalis, *Molecular diagnostics: for the clinical laboratorian.* Humana Press, 2nd ed., 2006.

[10] T. Chakraborty, *Charge migration in DNA: perspectives from physics, chemistry, and biology.* Springer, 2007.

[11] S. Roy, H. Vedala, A. D. Roy, D.-h. Kim, M. Doud, K. Mathee, H.-k. Shin, N. Shimamoto, V. Prasad, and W. Choi, "Direct electrical measurements on single-molecule genomic dna using single-walled carbon nanotubes," *Nano Letters*, vol. 8, no. 1, pp. 26–30, 2008. PMID: 18052084.

[12] M. Bockrath, N. Markovic, A. Shepard, M. Tinkham, L. Gurevich, L. P. Kouwenhoven, M. W. Wu, and L. L. Sohn, "Scanned conductance microscopy of carbon nanotubes and λ-dna," *Nano Letters*, vol. 2, no. 3, pp. 187–190, 2002.

[13] E. Braun, Y. Eichen, U. Sivan, and G. Ben-Yoseph, "DNA-templated assembly and electrode attachment of a conducting silver wire," *Nature*, vol. 391, pp. 775–778, Feb. 1998.

[14] C. Gómez-Navarro, F. Moreno-Herrero, P. J. de Pablo, J. Colchero, J. Gómez-Herrero, and A. M. Baró, "Contactless experiments on individual DNA molecules show no evidence for molecular wire behavior," *Proceedings of the National Academy of Science*, vol. 99, pp. 8484–8487, June 2002.

[15] D. H. Ha, H. Nham, K.-H. Yoo, H. mi So, H.-Y. Lee, and T. Kawai, "Humidity effects on the conductance of the assembly of dna molecules," *Chemical Physics Letters*, vol. 355, no. 5-6, pp. 405 – 409, 2002.

[16] T. Heim, D. Deresmes, and D. Vuillaume, "Conductivity of DNA probed by conducting-atomic force microscopy: Effects of contact electrode, DNA structure, and surface interactions," *Journal of Applied Physics*, vol. 96, pp. 2927–2936, Sept. 2004.

[17] H. Kleine, R. Wilke, C. Pelargus, K. Rott, A. Pühler, G. Reiss, R. Ros, and D. Anselmetti, "Absence of intrinsic electric conductivity in single ds-dna molecules," *Journal of Biotechnology*, vol. 112, no. 1-2, pp. 91 – 95, 2004. Physics of Single-Molecule Processes and Molecular Recognition in Organic Systems-Fundamental Interdisciplinary Research and its Consequences for Biotechnology.

[18] O. Legrand, D. Côte, and U. Bockelmann, "Single molecule study of dna conductivity in aqueous environment," *Phys. Rev. E*, vol. 73, p. 031925, Mar 2006.

[19] C. H. Lei, A. Das, M. Elliott, and J. E. MacDonald, "Conductivity of macromolecular networks measured by electrostatic force microscopy," *Applied Physics Letters*, vol. 83, pp. 482–+, July 2003.

[20] P. J. de Pablo, F. Moreno-Herrero, J. Colchero, J. Gómez Herrero, P. Herrero, A. M. Baró, P. Ordejón, J. M. Soler, and E. Artacho, "Absence of dc-conductivity in λ-dna," *Phys. Rev. Lett.*, vol. 85, pp. 4992–4995, Dec 2000.

[21] A. J. Storm, J. van Noort, S. de Vries, and C. Dekker, "Insulating behavior for DNA molecules between nanoelectrodes at the 100 nm length scale," *Applied Physics Letters*, vol. 79, pp. 3881–+, Dec. 2001.

[22] A. Terawaki, Y. Otsuka, H. Lee, T. Matsumoto, H. Tanaka, and T. Kawai, "Conductance measurement of a DNA network in nanoscale by point contact current imaging atomic force microscopy," *Applied Physics Letters*, vol. 86, pp. 113901–+, Mar. 2005.

[23] M. S. Xu, S. Tsukamoto, S. Ishida, M. Kitamura, Y. Arakawa, R. G. Endres, and M. Shimoda, "Conductance of single thiolated poly(GC)-poly(GC) DNA molecules," *Applied Physics Letters*, vol. 87, pp. 083902–+, Aug. 2005.

[24] Y. Zhang, R. H. Austin, J. Kraeft, E. C. Cox, and N. P. Ong, "Insulating behavior of λ-dna on the micron scale," *Phys. Rev. Lett.*, vol. 89, p. 198102, Oct 2002.

[25] H. Cohen, C. Nogues, R. Naaman, and D. Porath, "Direct measurement of electrical transport through single dna molecules of complex sequence," *Proceedings of the National Academy of Sciences of the United States of America*, vol. 102, no. 33, pp. 11589–11593, 2005.

[26] J. Gu, L. Cai, S. Tanaka, Y. Otsuka, H. Tabata, and T. Kawai, "Electric conductivity of dye modified DNA films with and without light irradiation in various humidities," *Journal of Applied Physics*, vol. 92, pp. 2816–2820, Sept. 2002.

[27] H. Nakayama, H. Ohno, and Y. Okahata, "Intramolecular electron conduction along dna strands and their temperature dependency in a dna-aligned cast film," *Chem. Commun.*, pp. 2300–2301, 2001.

[28] C. Nogues, S. R. Cohen, S. S. Daube, and R. Naaman, "Electrical properties of short dna oligomers characterized by conducting atomic force microscopy," *Phys. Chem. Chem. Phys.*, vol. 6, pp. 4459–4466, 2004.

[29] Y. Okahata, T. Kobayashi, K. Tanaka, and M. Shimomura, "Anisotropic Electric Conductivity in an Aligned DNA Cast Film," *Journal of the American Chemical Society*, vol. 120, pp. 6165–6166, June 1998.

[30] Y. Okahata, T. Kobayashi, H. Nakayama, and K. Tanaka, "Dna-aligned cast film and its anisotropic electron conductivity," *Supramolecular Science*, vol. 5, no. 3-4, pp. 317 – 320, 1998.

[31] D. Porath, A. Bezryadin, S. de Vries, and C. Dekker, "Direct measurement of electrical transport through DNA molecules," *Nature*, vol. 403, pp. 635–638, Feb. 2000.

[32] T. Shigematsu, K. Shimotani, C. Manabe, H. Watanabe, and M. Shimizu, "Transport properties of carrier-injected DNA," *Journal of Chemical Physics*, vol. 118, pp. 4245–4252, Mar. 2003.

[33] H.-W. Fink and C. Schönenberger, "Electrical conduction through DNA molecules," *Nature*, vol. 398, pp. 407–410, Apr. 1999.

[34] B. Hartzell, B. McCord, D. Asare, H. Chen, J. J. Heremans, and V. Soghomonian, "Current-voltage characteristics of diversely disulfide terminated λ-deoxyribonucleic acid molecules," *Journal of Applied Physics*, vol. 94, pp. 2764–2766, Aug. 2003.

[35] B. Hartzell, B. McCord, D. Asare, H. Chen, J. J. Heremans, and V. Soghomonian, "Comparative current-voltage characteristics of nicked and repaired λ-DNA," *Applied Physics Letters*, vol. 82, pp. 4800–+, June 2003.

[36] J. Hihath, B. Xu, P. Zhang, and N. Tao, "Study of single-nucleotide polymorphisms by means of electrical conductance measurements," *Proceedings of the National Academy of Science*, vol. 102, pp. 16979–16983, Nov. 2005.

[37] J. S. Hwang, S. W. Hwang, and D. Ahn, "Electrical conduction measurement of thiol modified dna molecules," *Superlattices and Microstructures*, vol. 34, no. 3-6, pp. 433 – 438, 2003. Proceedings of the joint 6th International Conference on New Phenomena in Mesoscopic Structures and 4th International Conference on Surfaces and Interfaces of Mesoscopic Devices.

[38] J. S. Hwang, K. J. Kong, D. Ahn, G. S. Lee, D. J. Ahn, and S. W. Hwang, "Electrical transport through 60 base pairs of poly(dG)-poly(dC) DNA molecules," *Applied Physics Letters*, vol. 81, pp. 1134–+, Aug. 2002.

[39] J. S. Hwang, G. S. Lee, K. J. Kong, D. J. Ahn, S. W. Hwang, and D. Ahn, "Electrical transport through poly(g)-poly(c) dna molecules," *Microelectronic Engineering*, vol. 63, no. 1-3, pp. 161 – 165, 2002.

[40] S. M. Iqbal, G. Balasundaram, S. Ghosh, D. E. Bergstrom, and R. Bashir, "Direct current electrical characterization of ds-DNA in nanogap junctions," *Applied Physics Letters*, vol. 86, pp. 153901–+, Apr. 2005.

[41] A. Rakitin, P. Aich, C. Papadopoulos, Y. Kobzar, A. S. Vedeneev, J. S. Lee, and J. M. Xu, "Metallic conduction through engineered dna: Dna nanoelectronic building blocks," *Phys. Rev. Lett.*, vol. 86, pp. 3670–3673, Apr 2001.

[42] P. Tran, B. Alavi, and G. Gruner, "Charge transport along the λ-dna double helix," *Phys. Rev. Lett.*, vol. 85, pp. 1564–1567, Aug 2000.

[43] Xu, Zhang, Li, and Tao, "Direct conductance measurement of single dna molecules in aqueous solution," *Nano Letters*, vol. 4, no. 6, pp. 1105–1108, 2004.

[44] K.-H. Yoo, D. H. Ha, J.-O. Lee, J. W. Park, J. Kim, J. J. Kim, H.-Y. Lee, T. Kawai, and H. Y. Choi, "Electrical conduction through poly(da)-poly(dt) and poly(dg)-poly(dc) dna molecules," *Phys. Rev. Lett.*, vol. 87, p. 198102, Oct 2001.

[45] Y. J. Yun, G. Park, S. Jung, and D. H. Ha, "Anomalous temperature dependence of electrical conductance of DNA-linked Au nanoparticle aggregates," *Applied Physics Letters*, vol. 88, pp. 063902–+, Feb. 2006.

[46] E. Meggers, M. E. Michel-Beyerle, and B. Giese, "Sequence dependent long range hole transport in dna," *Journal of the American Chemical Society*, vol. 120, no. 49, pp. 12950–12955, 1998.

[47] B. Giese, S. Wessely, M. Spormann, U. Lindemann, E. Meggers, and M. E. Michel-Beyerle, "On the mechanism of long-range electron transfer through dna," *Angewandte Chemie*, vol. 38, no. 7, pp. 996–998, 1999.

[48] C. J. Murphy, M. R. Arkin, Y. Jenkins, N. D. Ghatlia, S. H. Bossmann, N. J. Turro, and J. K. Barton, "Long-Range Photoinduced Electron Transfer Through a DNA Helix," *Science*, vol. 262, pp. 1025–1029, Nov. 1993.

[49] M. R. Arkin, E. D. A. Stemp, R. E. Holmlin, J. K. Barton, A. Hormann, E. J. C. Olson, and P. F. Barbara, "Rates of DNA-Mediated Electron Transfer between Metallointercalators," *Science*, vol. 273, pp. 475–480, July 1996.

[50] S. O. Kelley and J. K. Barton, "Electron Transfer Between Bases in Double Helical DNA," *Science*, vol. 283, pp. 375–+, Jan. 1999.

[51] R. G. Endres, D. L. Cox, and R. R. Singh, "Colloquium: The quest for high-conductance DNA," *Reviews of Modern Physics*, vol. 76, pp. 195–214, Jan. 2004.

[52] K. W. Hipps, "It's all about contacts," *Science*, vol. 294, no. 5542, pp. 536–537, 2001.

[53] A. Kuzyk, *Molecular Devices for Nanoelectronics And Plasmonics*. PhD thesis, University of Jyväskylä, 2009.

[54] N. C. Seeman, "DNA in a material world," *Nature*, vol. 421, pp. 427–431, Jan. 2003.

[55] N. C. Seeman, "Nucleic acid junctions and lattices," *Journal of Theoretical Biology*, vol. 99, no. 2, pp. 237 – 247, 1982.

[56] N. R. Kallenbach, R. Ma, and N. C. Seeman, "An immobile nucleic acid junction constructed from oligonucleotides," *Nature*, vol. 305, pp. 829–831, Oct. 1983.

[57] E. Winfree, F. Liu, L. A. Wenzler, and N. C. Seeman, "Design and self-assembly of two-dimensional DNA crystals," *Nature*, vol. 394, pp. 539–544, Aug. 1998.

[58] S. H. Park, R. Barish, H. Li, J. H. Reif, G. Finkelstein, H. Yan, and T. H. LaBean, "Three-helix bundle dna tiles self-assemble into 2d lattice or 1d templates for silver nanowires," *Nano Letters*, vol. 5, no. 4, pp. 693–696, 2005.

[59] H. Yan, S. H. Park, G. Finkelstein, J. H. Reif, and T. H. LaBean, "DNA-Templated Self-Assembly of Protein Arrays and Highly Conductive Nanowires," *Science*, vol. 301, pp. 1882–1884, Sept. 2003.

[60] C. Mao, W. Sun, and N. C. Seeman, "Designed two-dimensional dna holliday junction arrays visualized by atomic force microscopy," *Journal of the American Chemical Society*, vol. 121, no. 23, pp. 5437–5443, 1999.

[61] T. H. LaBean, H. Yan, J. Kopatsch, F. Liu, E. Winfree, J. H. Reif, and N. C. Seeman, "Construction, analysis, ligation, and self-assembly of dna triple crossover complexes," *Journal of the American Chemical Society*, vol. 122, no. 9, pp. 1848–1860, 2000.

[62] S. H. Park, P. Yin, Y. Liu, J. H. Reif, T. H. LaBean, and H. Yan, "Programmable dna self-assemblies for nanoscale organization of ligands and proteins," *Nano Letters*, vol. 5, no. 4, pp. 729–733, 2005.

[63] X. Li, X. Yang, J. Qi, and N. C. Seeman, "Antiparallel dna double crossover molecules as components for nanoconstruction," *Journal of the American Chemical Society*, vol. 118, no. 26, pp. 6131–6140, 1996.

[64] P. W. K. Rothemund, "Folding DNA to create nanoscale shapes and patterns," *Nature*, vol. 440, pp. 297–302, Mar. 2006.

[65] Q. Gu, C. Cheng, R. Gonela, S. Suryanarayanan, S. Anabathula, K. Dai, and D. T. Haynie, "Dna nanowire fabrication," *Nanotechnology*, vol. 17, no. 1, p. R14, 2006.

[66] J. Sharma, Y. Ke, C. Lin, R. Chhabra, Q. Wang, J. Nangreave, Y. Liu, and H. Yan, "Dna-tile-directed self-assembly of quantum dots into two-dimensional nanopatterns," *Angewandte Chemie International Edition*, vol. 47, no. 28, pp. 5157–5159, 2008.

[67] M. G. Warner and J. E. Hutchison, "Linear assemblies of nanoparticles electrostatically organized on DNA scaffolds," *Nature Materials*, vol. 2, pp. 272–277, Apr. 2003.

[68] J. Zheng, P. E. Constantinou, C. Micheel, A. P. Alivisatos, R. A. Kiehl, and N. C. Seeman, "Two-dimensional nanoparticle arrays show the organizational power of robust dna motifs," *Nano Letters*, vol. 6, no. 7, pp. 1502–1504, 2006.

[69] J. D. Le, Y. Pinto, N. C. Seeman, K. Musier-Forsyth, T. A. Taton, and R. A. Kiehl, "DNA-Templated Self-Assembly of Metallic Nanocomponent Arrays on a Surface," *Nano Letters*, vol. 4, pp. 2343–2347, Dec. 2004.

[70] J. Zhang, Y. Liu, Y. Ke, and H. Yan, "Periodic Square-Like Gold Nanoparticle Arrays Templated by Self-Assembled 2D DNA Nanogrids on a Surface," *Nano Letters*, vol. 6, pp. 248–251, Feb. 2006.

[71] J. Sharma, R. Chhabra, Y. Liu, Y. Ke, and H. Yan, "Dna-templated self-assembly of two-dimensional and periodical gold nanoparticle arrays," *Angewandte Chemie International Edition*, vol. 45, no. 5, pp. 730–735, 2006.

[72] K. Keren, R. S. Berman, E. Buchstab, U. Sivan, and E. Braun, "Dna-templated carbon nanotube field-effect transistor," *Science*, vol. 302, no. 5649, pp. 1380–1382, 2003.

[73] H. T. Maune, S. Han, R. D. Barish, M. Bockrath, I. Goddard, W. A., P. W. K. Rothemund, and E. Winfree, "Self-assembly of carbon nanotubes into two-dimensional geometries using DNA origami templates," *Nature Nanotechnology*, vol. 5, pp. 61–66, Jan. 2010.

[74] K. Keren, M. Krueger, R. Gilad, G. Ben-Yoseph, U. Sivan, and E. Braun, "Sequence-Specific Molecular Lithography on Single DNA Molecules," *Science*, vol. 297, pp. 72–75, July 2002.

[75] R. Chhabra, J. Sharma, Y. Ke, Y. Liu, S. Rinker, S. Lindsay, and H. Yan, "Spatially addressable multiprotein nanoarrays templated by aptamer-tagged dna nanoarchitectures," *Journal of the American Chemical Society*, vol. 129, no. 34, pp. 10304–10305, 2007.

[76] A. Kuzyk, K. T. Laitinen, and P. Törmä, "Dna origami as a nanoscale template for protein assembly," *Nanotechnology*, vol. 20, no. 23, p. 235305, 2009.

[77] J. Sharma, R. Chhabra, C. S. Andersen, K. V. Gothelf, H. Yan, and Y. Liu, "Toward reliable gold nanoparticle patterning on self-assembled dna nanoscaffold," *Journal of the American Chemical Society*, vol. 130, no. 25, pp. 7820–7821, 2008.

[78] A. Castellanos, A. Ramos, A. González, N. G. Green, and H. Morgan, "Electrohydrodynamics and dielectrophoresis in microsystems: scaling laws," *Journal of Physics D: Applied Physics*, vol. 36, no. 20, p. 2584, 2003.

[79] M. Washizu and O. Kurosawa, "Electrostatic manipulation of dna in micro-fabricated structures," *Industry Application*, vol. 26, no. 6, 1990.

[80] M. Washizu, O. Kurosawa, I. Arai, S. Suzuki, and N. Shimamoto, "Applications of electrostatic stretch-and-positioning of dna," *Industry Application*, vol. 31, no. 3, 1995.

[81] S. Suzuki, T. Yamanashi, S. Tawaza, O. Kurosawa, and M. Washizu, "Quantitative analysis of dna orientation in stationary ac electric fields using fluorescence anisotropy," *Industry Application*, vol. 34, no. 1, 1998.

[82] S. Tsukahara, K. Yamanaka, and H. Watarai, "Dielectrophoretic behavior of single dna in planar and capillary quadrupole microelectrodes," *Chemistry Letters*, vol. 30, no. 3, pp. 250–251, 2001.

[83] D. J. G. Bakewell, M. P. Hughes, J. J. Milner, and H. Morgan, "Dielectrophoretic manipulation of avidin and dna," Engineering in Medicine and Biology Society, 1998.

[84] V. Namasivayam, R. G. Larson, D. T. Burke, and M. A. Burns, "Electrostretching dna molecules using polymer- enhanced media within microfabricated devices," *Analytical Chemistry*, vol. 74, no. 14, pp. 3378–3385, 2002.

[85] S. Tuukkanen, A. Kuzyk, J. J. Toppari, V. P. Hytönen, T. Ihalainen, and P. Törmä, "Dielectrophoresis of nanoscale double-stranded DNA and humidity effects on its electrical conductivity," *Applied Physics Letters*, vol. 87, pp. 183102–+, Oct. 2005.

[86] C. L. Asbury, A. H. Diercks, and G. van den Engh, "Trapping of dna by dielectrophoresis," *Electrophoresis*, vol. 23, no. 16, pp. 2658–2666, 2002.

[87] D. J. Bakewell, I. Ermolina, H. Morgan, J. Milner, and Y. Feldman, "Dielectric relaxation measurements of 12 kbp plasmid dna," *Biochimica et Biophysica Acta (BBA) - Gene Structure and Expression*, vol. 1493, no. 1-2, pp. 151 – 158, 2000.

[88] C. Chou, J. Tegenfeldt, O. Bakajin, S. Chan, E. Cox, N. Darnton, T. Duke, and R. Austin, "Electrodeless Dielectrophoresis of Single- and Double-Stranded DNA," *Biophysical Journal*, vol. 83, pp. 2170–2179, Oct. 2002.

[89] S. Tuukkanen, J. J. Toppari, A. Kuzyk, L. Hirviniemi, V. P. Hytönen, T. Iha-
lainen, and P. Törmä, "Carbon nanotubes as electrodes for dielectrophoresis
of dna," *Nano Letters*, vol. 6, no. 7, pp. 1339–1343, 2006.

[90] S. Tuukkanen, A. Kuzyk, J. J. Toppari, H. Häkkinen, V. P. Hytönen, E. Niska-
nen, M. Rinkiö, and P. Törmä, "Trapping of 27 bp-8 kbp dna and immobiliza-
tion of thiol-modified dna using dielectrophoresis," *Nanotechnology*, vol. 18,
no. 29, p. 295204, 2007.

[91] H. Häkkinen, M. Walter, and H. Grönbeck, "Divide and protect: Capping
gold nanoclusters with molecular gold-thiolate rings," *The Journal of Physical
Chemistry B*, vol. 110, no. 20, pp. 9927–9931, 2006. PMID: 16706449.

[92] J. Macdonald and E. Barsoukov, *Impedance Spectroscopy: Theory, Experi-
ment, And Applications.* Wiley, New Jersey, 2005.

[93] C. Longo, A. F. Nogueira, M.-A. De Paoli, and H. Cachet, "Solid-state and
flexible dye-sensitized tio2 solar cells: a study by electrochemical impedance
spectroscopy," *The Journal of Physical Chemistry B*, vol. 106, no. 23,
pp. 5925–5930, 2002.

[94] Q. Wang, J.-E. Moser, and M. Grätzel, "Electrochemical impedance spectro-
scopic analysis of dye-sensitized solar cells," *The Journal of Physical Chemistry
B*, vol. 109, no. 31, pp. 14945–14953, 2005.

[95] M. Glatthaar, M. Riede, N. Keegan, K. Sylvester-Hvid, B. Zimmermann,
M. Niggemann, A. Hinsch, and A. Gombert, "Efficiency limiting factors of
organic bulk heterojunction solar cells identified by electrical impedance spec-
troscopy," *Solar Energy Materials and Solar Cells*, vol. 91, no. 5, pp. 390 –
393, 2007. Selected Papers from the European Conference on Hybrid and Or-
ganic Solar Cells – ECHOS '06, European Conference on Hybrid and Organic
Solar Cells.

[96] J. Macdonald, "Impedance spectroscopy," *Annals of Biomedical Engineering*,
vol. 20, pp. 289–305, 1992. 10.1007/BF02368532.

[97] G. Ragoisha, N. Osipovich, A. Bondarenko, J. Zhang, S. Kocha, and A. Iiyama,
"Characterisation of the electrochemical redox behaviour of pt electrodes by
potentiodynamic electrochemical impedance spectroscopy," *Journal of Solid*

State Electrochemistry, vol. 14, pp. 531–542, 2010. 10.1007/s10008-008-0663-7.

[98] J. Scully, D. Silverman, and M. Kendig, *Electrochemical impedance: analysis and interpretation.* American Society of Testing and Materials, 1993.

[99] "3 and 4 electrode configurations." `http://www.novocontrol.de/html/intro_4wire.htm`.

[100] J. J. Roberts and J. A. Tyburczy, "Impedance spectroscopy of single and polycrystalline olivine: Evidence for grain boundary transport," *Physics and Chemistry of Minerals*, vol. 20, pp. 19–26, 1993. 10.1007/BF00202246.

[101] V. Lvovich and M. Smiechowski, "Ac impedance investigation of conductivity of automotive lubricants using two- and four-electrode electrochemical cells," *Journal of Applied Electrochemistry*, vol. 39, pp. 2439–2452, 2009. 10.1007/s10800-009-9933-z.

[102] V. S. Bagotskii, *Fundamentals of Electrochemistry.* Wiley, 2005.

[103] J. U. Kim, "Electrical double layer: revisit based on boundary conditions," *ArXiv Physics e-prints*, Nov. 2005.

[104] B. J. Kirby, *Micro- and Nanoscale Fluid Mechanics: Transport in Microfluidic Devices.* Cambridge University Press, 2010.

[105] W. B. Russel, D. A. Saville, and W. R. Schowalter, *Colloidal Dispersions.* Cambridge University Press, 1989.

[106] A. D. McNaught and A. Wilkinson, *IUPAC. Compendium of Chemical Terminology, 2nd edition.* Blackwell Scientific Publications, Oxford, 1997.

[107] J. O. Bockris, A. K. N. Reddy, and G.-A. Maria, *Modern Electrochemistry 2A. Fundamentals of Electrodics.* Kluwer Academic/Plenum Publishers, 2000.

[108] C.-H. Kim, S.-I. Pyun, and J.-H. Kim, "An investigation of the capacitance dispersion on the fractal carbon electrode with edge and basal orientations," *Electrochimica Acta*, vol. 48, no. 23, pp. 3455 – 3463, 2003.

[109] C. A. Schiller and W. Strunz, "The evaluation of experimental dielectric data of barrier coatings by means of different models," *Electrochimica Acta*, vol. 46, no. 24-25, pp. 3619 – 3625, 2001.

[110] J.-B. Jorcin, M. E. Orazem, N. Pébère, and B. Tribollet, "Cpe analysis by local electrochemical impedance spectroscopy," *Electrochimica Acta*, vol. 51, no. 8-9, pp. 1473 – 1479, 2006. Electrochemical Impedance Spectroscopy - Selection of papers from the 6th International Symposium (EIS 2004) 16-21 May 2004, Cocoa Beach, FL, USA.

[111] J. Bisquert and A. Compte, "Theory of the electrochemical impedance of anomalous diffusion," *Journal of Electroanalytical Chemistry*, vol. 499, no. 1, pp. 112 – 120, 2001.

[112] D. R. Franceschetti, J. R. Macdonald, and R. P. Buck, "Interpretation of finite-length-warburg-type impedances in supported and unsupported electrochemical cells with kinetically reversible electrodes," *Journal of The Electrochemical Society*, vol. 138, no. 5, pp. 1368–1371, 1991.

[113] D. R. Franceschetti and J. R. Macdonald, "Diffusion of neutral and charged species under smallsignal a.c. conditions," *J. Electroanat. Chem.*, vol. 101, no. 101, pp. 307–316.

[114] B.-L. S. Instruments, "Handbook of electrochemical impedance spectroscopy." `http://www.bio-logic.info/potentiostat/notesheis.html`.

[115] V. Linko, "Dielectrophoresis of thiol-modified dna origami," Master's thesis, University of Jyväskylä, 2007.

[116] V. Linko, "Erittäin pienten elektrodien valmistus dna:n immobilisoimiseksi." Special Assignment, University of Jyväskylä, 2007.

[117] H. Li, S. H. Park, J. H. Reif, T. H. LaBean, and H. Yan, "Dna-templated self-assembly of protein and nanoparticle linear arrays," *Journal of the American Chemical Society*, vol. 126, no. 2, pp. 418–419, 2004. PMID: 14719910.

[118] M. Zuker, "Mfold web server for nucleic acid folding and hybridization prediction," *Nucleic Acids Research*, vol. 31, no. 13, pp. 3406–3415, 2003.

[119] V. Linko, J. Leppiniemi, S.-T. Paasonen, V. P. Hytönen, and J. J. Toppari, "Defined-size dna triple crossover construct for molecular electronics: modification, positioning and conductance properties," *Nanotechnology*, vol. 22, no. 27, p. 275610, 2011.

[120] A. Kuzyk, B. Yurke, J. J. Toppari, V. Linko, and P. Törmä, "Dielectrophoretic trapping of dna origami," *Small*, vol. 4, no. 4, pp. 447–450, 2008.

[121] V. Linko, S.-T. Paasonen, A. Kuzyk, P. Törmä, and J. J. Toppari, "Characterization of the conductance mechanisms of dna origami by ac impedance spectroscopy," *Small*, vol. 5, no. 21, pp. 2382–2386, 2009.

[122] M. Briman, N. P. Armitage, E. Helgren, and G. GrÃ¼ner, "Dipole relaxation losses in dna," *Nano Letters*, vol. 4, no. 4, pp. 733–736, 2004.

[123] J. R. Macdonald, "How to get the levm/levmw -version 8.10 program, complex nonlinear least squares fitting program." `http://www.jrossmacdonald.com/levminfo.html`.

[124] C. Yamahata, D. Collard, T. Takekawa, M. Kumemura, G. Hashiguchi, and H. Fujita, "Humidity dependence of charge transport through dna revealed by silicon-based nanotweezers manipulation," *Biophysical Journal*, vol. 94, no. 1, pp. 63 – 70, 2008.

[125] L. Burke and P. Nugent, "The electrochemistry of gold: I the redox behaviour of the metal in aqueous media," *Gold Bulletin*, vol. 30, pp. 43–53, 1997. 10.1007/BF03214756.

[126] A. Toro-Labbé, *Theoretical aspects of chemical reactivity*. Elsevier, 2007.

[127] W. T. Wallace, R. B. Wyrwas, R. L. Whetten, R. Mitrić, and V. Bonacić-Koutecký, "Oxygen adsorption on hydrated gold cluster anions: Experiment and theory," *Journal of the American Chemical Society*, vol. 125, no. 27, pp. 8408–8414, 2003. PMID: 12837115.

[128] J. H. Anderson and G. A. Parks, "Electrical conductivity of silica gel in the presence of adsorbed water," *The Journal of Physical Chemistry*, vol. 72, no. 10, pp. 3662–3668, 1968.

[129] B. Xu and N. J. Tao, "Measurement of Single-Molecule Resistance by Repeated Formation of Molecular Junctions," *Science*, vol. 301, pp. 1221–1223, Aug. 2003.

[130] S. Liu, *Conductance of individual DNA molecules measured with adjustable break junctions*. PhD thesis, University of Konstanz, 2010.

[131] R. L. Wells and T. F. Jr., "Adsorption of water on clean gold by measurement of work function changes," *Surface Science*, vol. 32, no. 3, pp. 554 – 560, 1972.

[132] M. R. Wright, *An introduction to aqueous electrolyte solutions.* John Wiley and Sons, 2007.

[133] J. Freund, J. Halbritter, and J. Hörber, "How dry are dried samples? water adsorption measured by stm," *Microscopy Research and Technique*, vol. 44, no. 5, pp. 327–338, 1999.

[134] Q.-H. Wan, "Effect of electrical double-layer overlap on the electroosmotic flow in packed-capillary columns," *Analytical Chemistry*, vol. 69, no. 3, pp. 361–363, 1997.

[135] T. Kleine-Ostmann, C. Jördens, K. Baaske, T. Weimann, M. H. de Angelis, and M. Koch, "Conductivity of single-stranded and double-stranded deoxyribose nucleic acid under ambient conditions: The dominance of water," *Applied Physics Letters*, vol. 88, pp. 102102–+, Mar. 2006.

[136] I. Benjamin, D. Evans, and A. Nitzan, "Electron tunneling through water layers: Effect of layer structure and thickness," *The Journal of Chemical Physics*, vol. 106, pp. 6647–6654, Apr. 1997.

[137] W. Schmickler, "Tunneling of electrons through thin layers of water," *Surface Science*, vol. 335, pp. 416 – 421, 1995. Proceedings of the IUVSTA Workshop on Surface Science and Electrochemistry.

[138] A. Mosyak, P. Graf, I. Benjamin, and A. Nitzan, "Electron tunneling through water layers: Effect of polarizability," *The Journal of Physical Chemistry A*, vol. 101, no. 4, pp. 429–433, 1997.

[139] Y. A. Hong, J. R. Hahn, and H. Kang, "Electron transfer through interfacial water layer studied by scanning tunneling microscopy," *The Journal of chemical physics*, vol. 108, pp. 4367–4370, Mar. 1998.

[140] I. Rungger, X. Chen, U. Schwingenschlögl, and S. Sanvito, "Finite-bias electronic transport of molecules in a water solution," *Phys. Rev. B*, vol. 81, p. 235407, Jun 2010.

[141] N. Nandi, K. Bhattacharyya, and B. Bagchi, "Dielectric relaxation and solvation dynamics of water in complex chemical and biological systems," *Chemical Reviews*, vol. 100, no. 6, pp. 2013–2046, 2000.

[142] R. N. Barnett, C. L. Cleveland, A. Joy, U. Landman, and G. B. Schuster, "Charge Migration in DNA: Ion-Gated Transport," *Science*, vol. 294, pp. 567–571, Oct. 2001.

[143] S.-P. Liu, S. Weisbrod, Z. Tang, A. Marx, E. Scheer, and A. Erbe, "Direct measurement of electrical transport through g-quadruplex dna with mechanically controllable break junction electrodes," *Angewandte Chemie International Edition*, vol. 49, no. 19, pp. 3313–3316, 2010.

[144] B. Bornemann, S.-P. Liu, A. Erbe, E. Scheer, and A. Marx, "Thiolated nucleotides for immobilisation of dna oligomers on gold surfaces," *ChemPhysChem*, vol. 9, no. 9, pp. 1241–1244, 2008.

Appendix A

Parameters used in
the lithography process

Thermal growing of SiO2

- Wafers were cut into 3 pieces to fit the wafer into the oxidation tube, and carefully cleaned to clear impurities and organic dirt.

- Growth was done in a temperature of 1100 ºC overnight with a slow oxygen flow (few bubbles per second in water).

- Heating up took 4 hours and cooling down 8 hours.

- During the heating and cooling processes oxygen flow was off and nitrogen flow was used instead.

- The oxidized pieces were again cleared and stored for later use.

- The thickness of the resulting oxide layer is about 700-900 nm.

Deposition of the resist

- A small chip was carefully cut from the oxidized wafer and cleaned in hot acetone and rinsed with IPA.

- The chip was put on the spinner (vacuum was used to immobilize the chip). One drop of the resist was then deposited on the chip.

- The resist used was Microchem PMMA 950 in anisole. The original product was 11%, but it was diluted to 2%.

- 2000 RPM was used with sufficiently low acceleration. The resist layer seemed to saturate around 30 seconds, but we used 45 seconds just to be sure.

- The resulting resist layer was about 100 nm thick.

Exposure

- First latex balls or silver paint was added on the chip (near the edge of the chip) for rough focusing.

- The electron beam writer used for patterning was Raith E-line, i.e. a tool based on SEM and especially designed for e-beam patterning.

- After the loading procedure and the rough focusing contamination spots were burned with 10 μm aperture. A round shape and a diameter of 13-20 nm was required from the beam before exposure.

- Before the exposure the current of the beam was measured.

- Inner structures (i.e. the fingertips, smaller parts of the electrodes – area of 10×10 μm^2) were exposed by using the 10 μm aperture. Step size used was 24 nm for the area-like parts (rasterized with 2 parallel lines or more) of the electrode. The tip of the electrode was realized as a single pixel line and the step size for it was 0.2 nm. The doses were around 400 μAs/cm^2 and 4000 pAs/cm, respectively. The current was about 0.037 nA.

- Middle parts (area of 120x120 μm^2) were also exposed using the 10 μm aperture, but the step size was increased to 64 nm.

- Outer structures (i.e. pads, larger parts of the electrodes – two areas of 2x2 mm^2) were exposed using 120 μm aperture, while the step size was about 220 nm. Current was 5-7 nA depending on the age of the filament.

Etching processes

- The RIE used was Oxford Plasmalab 80+.

- The cleaning of the organic residues from the developed areas was done with the following parameters: oxygen flow 50 sccm, RF power 15 W, time 10 s, pressure 30 mTorr.

- The recipe of the cleaning before DEP experiments: oxygen flow 50 sccm, RF power 25 W, time 1 min, pressure 40 mTorr.

Metallization

- The evaporation rates were measured using a rate meter based on a quartz crystal microbalance.

- Evaporation of titanium happened with a rate of about 0.2 nm/s.

- The evaporation rate of gold was about 0.04-0.06 nm/s.

Appendix B

Details for design and fabrication of the TX tile B-A-B complex

Below are the base sequences (and colors) of the strands in the figure B.1:

1. ATCGAGAGAC ATAACTGCTT GACCACGCTG TATCGGAACC TGACTCCTAA TCAGCA

2. AGGAGTCACT CTCGATGCCA GACG

3. GGTATAGTAT GCAACGTGAA TGAACAAGGT GAGGTGTCAA TGGAGATGAA TGTTC

4. ATCTCCATTG ACAGGTCAAG CAGTTATGTG GTTCTGCATA CTATACCGAA TGTTC

5. ATAGCACCAC TGCAAGGCCA GACG

6. CTTGCAGTCC TTGTTCATTC ACGTCGATAC AGCGTCCTCA GGTGCTATAA TCAGCA

7. TGGAGCGACA TG with 5' thiol modification

8. AGATAACATA AGGACACTTA GGAATCCAGT ACTGACACAC AGTTGGAACA TTC

9. CAACTGTGTG AATGGGACTT TGCTGATT (28)

10. AGCTGAACCT ACAGTCATAC GACTCGAACA CGTAGTATCA TCTAGCGTCT GGC

11. CTAGATGATA CTACGGCTAC TCAGTACTGG ATTCCTAAGT GAATTGGAC

12. GATCATGATG TTCGAGTCGT ATGACTGTAC TATCTCCTTA TGTTATCTCA TGTCGCTCCA

13. AAGTCCCATT GTAGCTCATG ATCGTCCAAT TGATAGCCCT GTTGACATGT CGCTCCA

14. TCAACAGGGG GTTCAGCTCA TGTCGCTCCA

The thiol modification used was not the typical C6-thiol of the figure 1.10. Instead, the molecule used, /5ThioMC6-D/, is shown in the figure B.2. The S-S bond is weaker than the S-Au bond and thus the S-S bond opens when the linker meets gold and S-Au bond is formed (after which the molecule is similar to the C6-thiol). This kind of S-S linker protection prevents aggregation of the molecules.
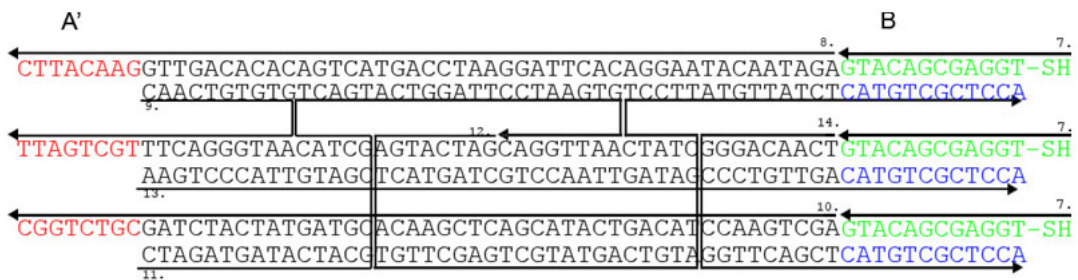
Figure B.1: *Arrows indicate the direction from 5' to 3' end. A and A' are complementary sticky ends and B is the thiol-modified sticky end. One can follow one of the strands to see how the tile, and especially crossovers, form.*
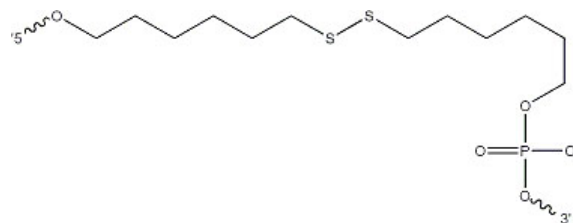

Figure B.2: *The thiol modification used in 5' ends of both the B-A-B complexes and the origami structures.*

Each strand was modified separately by adding 1.5 μl of master mix (see table B.1) to tubes containing 10 μl of strands of tile A (10 μM) or by adding 3.0 μl of master mix to tubes containing 20 μl of strands of tile B (10 μM). The strand 7 was diluted to the same concentration (8.7 μM) as the other strands had after incubation with T4 kinase.

Table B.1: *Amounts of components used in the master mix for the kinase treatment and the reaction solution.*

Component	Amount [μl]
Master mix	
40 mM Tris, 1 mM EDTA, 19 mM HAc, 500 mM MgAc	5.8
40 mM Tris, 1 mM EDTA, 19 mM HAc	0.8
10× T4 DNA Ligase reaction buffer	23.0
T4 Polynucleotide Kinase (10,000 U/ml)	0.5
Reaction solution	
All B-A-B complex strands (pretreated with master mix) (in total)	260.0
40 mM Tris, 1 mM EDTA, 19 mM HAc, 500 mM MgAc	1.0
40 mM Tris, 1 mM EDTA, 19 mM HAc	7.0
10× T4 DNA Ligase reaction buffer	30.0
T4 DNA Ligase (400,000 U/ml)	2.0

Appendix C

Details for design and fabrication of the origami structures

Base sequences of the thiol-modified side strands for one end:

- 5' AGCATAAAGCTAAATC CTCTCTCT CTCTCTCT CTCTCTCT CTCTCTCT /3ThioMC3-D/ 3'

- 5' /5ThioMC6-D/ CTCTCTCT CTCTCTCT CTCTCTCT CTCTCTCT CTGTAGCTCAACATGT 3'

and for another

- 5' /5ThioMC6-D/ CTCTCTCT CTCTCTCT CTCTCTCT CTCTCTCT CGACAAAAGGTAAAGT 3'

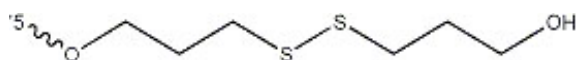- 5' AAATCAGATATAGAAG CTCTCTCT CTCTCTCT CTCTCTCT CTCTCTCT /3ThioMC3-D/ 3'

Figure C.1: *The thiol modification used in 3' ends (with origami structures).*

16 bases of each strand are complementary with M13mp18 DNA sequence on the edges of the origami, and a 32-bases-long repetitive CT sequence is used as a spacer between the origami structure and the thiols. The linker molecule /5ThioMC6-D/ is presented in the figure B.2 of the appendix B. Figure C.1 shows the 3' end version of the same S-S linker.

Table C.1 shows the amounts of components used in the fabrication and ligation procedures and figure C.2 is a schematic presentation of the design.
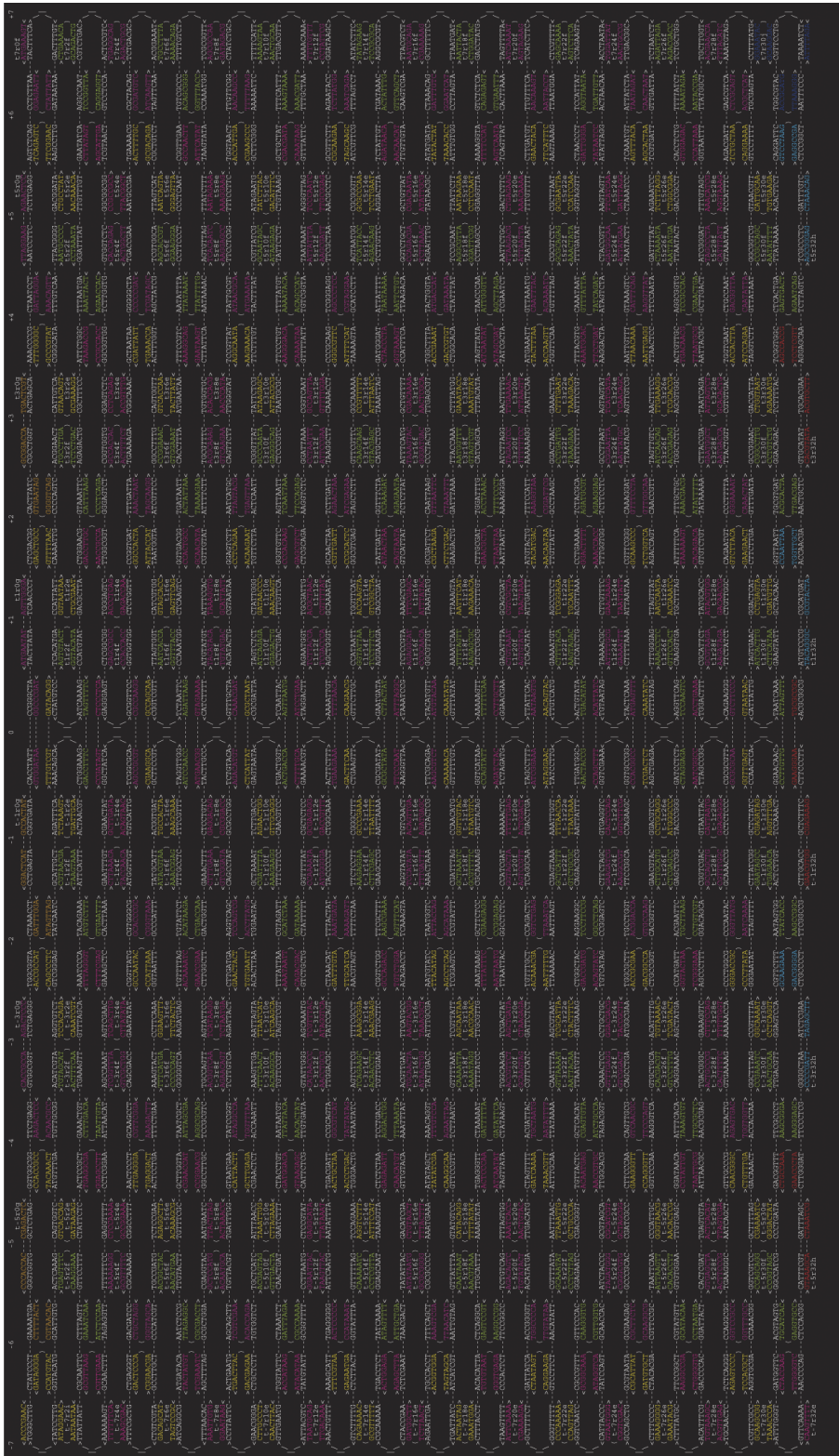
Figure C.2: *A schematic presentation of the design of a rectangular DNA origami.*

Table C.1: *The amounts of components (in the order of mixing) used in the origami fabrication and the ligation procedure followed by the annealing.*

Component	Amount [μl]
Origami fabrication	
10× TAE Mg++ buffer	5.0
Distilled water	19.7
10× T4 DNA Ligase reaction buffer	5.0
M13mp18 virus (0.93 nM)	5.4
Staple strand mix (0.78 μM)	6.9
Thiol-modified side strands (1 μM)	5.0
T4 Polynucleotide kinase	3.0
Ligation procedure	
Distilled water	67.0
10× TAE Mg++ buffer	9.0
10× T4 DNA Ligase reaction buffer	9.0
Annealed DNA origami solution	10.0
T4 DNA Ligase	5.0

Appendix D

The filtration/buffer exchange procedure

The origami solution was not diluted before spinning, whereas the TX tile solution was diluted 1:10 to the DEP buffer. For filtering and buffer exchange we used Millipore Microcon YM-100 spin filters which have a MW cutoff of 100 kDa. The procedure was done in the following way:

- 100 μL of the sample was mixed with 300 μL of the DEP buffer and put into the YM spin filter.

- Sample was spun for 12 min at 1000 relative centrifugal force (rcf) and 4 ºC.

- After that the sample was removed from the centrifuge. The filter had only a few tens of microliters of sample left in it. The filter was taken out and the liquid in the tube below was removed. Then the filter was reinserted and 400 μL of the buffer was added.

- Sample was spun for 7 min at the same conditions. This left us with 100 μL of sample retained in the spin filter.

- Finally, the spin filter was removed, placed upside down in a fresh tube and spun in a microcentrifuge for 2-3 min to collect the solution.

The 100 kDa MW cutoff was not sufficient in the case of the TX tile structures since only tile A has a MW smaller than 100 kDa, which means that most of the non-bonded (via sticky-end pairing) tiles B and complexes B-A remained in the solution instead of filtering out lowering the overall yield of the trapping procedure.

Appendix E

Typical measuring parameters used in the AC measurements

Table E.1: *Typical parameters used in the AC measurements for three different frequency ranges: high (∼ 1 Hz-100 kHz), middle (∼ 0.5-5 Hz), and low (∼ 0.01-1 Hz).*

Parameter	High	Middle	Low
Measuring interval [ms]	200	300	300
Maximum deviation (noise) [%]	1	0.1	0.01
Averaging [scans/point]	100	100	100
Maximum iterations	200	300	400
(tries to meet the deviation condition)			
Time constants to measure over:	20	15	10
Number of data points (logarithmic steps):	25	20	15
Slope of the low-pass filter [dB/octave]:	18	18	12

The lowest frequencies measured were determined by the quality of the measured data. When the total impedance of the system approached 10 GΩ (i.e. the input impedance of the preamplifiers) the data started to look quite distorted.